Old Dominion University

ODU Digital Commons

Summer 2005

Modeling and Simulation of Silicon Photonic Crystals Effect of Oxidation and Etching

G. M. Haider Ali
Old Dominion University

Follow this and additional works at: https://digitalcommons.odu.edu/ece_etds

 Part of the Computational Engineering Commons, and the Electrical and Computer Engineering Commons

MODELING AND SIMULATION OF SILICON PHOTONIC CRYSTALS: EFFECT OF OXIDATION AND ETCHING

By

G. M. Haider Ali

B.S.E.E. March 2002,

Bangladesh University of Engineering and Technology (BUET)

A Thesis Submitted to the Faculty of

Old Dominion University in Partial Fulfillment of the

Requirements for the Degree of

MASTER OF SCIENCE

ELECTRICAL ENGINEERING

OLD DOMINION UNIVERSITY

August 2005

Approved by:

_____

Dr. Sacharia Albin (Director)

_____

Dr. Mohamed Karim (Member)

_____

Dr. Vijayan Asari (Member)

ABSTRACT

MODELING AND SIMULATION OF SILICON PHOTONIC CRYSTALS: EFFECT OF OXIDATION AND ETCHING

G. M. Haider Ali

Old Dominion University, 2005

Director: Dr. Sacharia Albin

Recent inventions of a silicon Raman laser and a high speed photon modulator might motivate integration of electronic and photonic active devices on the same silicon chip. Passive photonic devices in silicon such as waveguides, couplers and splitters have been developed. Photonic devices must be compatible with standard silicon CMOS fabrication processing in order to achieve the integration. Since CMOS fabrication involves a myriad of process steps, it is important to study the effect of processing on photonic devices. Oxidation and etching, two fundamental processes in silicon technology, are utilized in this thesis to model their effects on silicon photonic crystals. Triangular and square lattices made of both air holes and silicon pillars are employed. The photonic band structures of these lattices are analyzed before and after oxidation and oxide etching. It is found that the width of the band gap and the midgap frequency can be varied systematically using oxidation and etching. Another interesting result is that the band gap tuning does not follow the same path for both oxidation and etching. This is a direct result of the change in silicon filling ratio during oxidation, which is unaffected by oxide etching. Thus the results of this thesis show a very flexible method in tuning the band gap of silicon photonic crystals.

The results are further validated using frequency tuning of a single defect cavity in a silicon photonic crystal of square lattice. Plane Wave Expansion Method is used to calculate necessary band structures and a Finite Difference Time Domain (FDTD) based software is used to find the frequency spectrum of the single defect.

This thesis is dedicated to my mother and late father,
who's endless efforts and wishes inspire my way.

ACKNOWLEDGMENTS

First and foremost, I would like to thank God for giving me the strength and ability to accomplish this task.

Secondly, I would like to thank my advisor, Dr. Sacharia Albin for giving me the confidence to complete this goal. His wisdom, encouragement, and his patience have been very important for this research. I would also like to thank Dr. Mohammad Karim and Dr. Vijayan Asari for serving as my thesis committee members and taking time away from their busy schedule to help me bring this research to a close. Very special mentions go to Dr. Shangping Guo and Feng Wu. Their experiences, knowledge in photonics, and kind guidance were most valuable and often ingenious. I would also like to acknowledge my colleagues, Kurt Peters, Khaled Ikram, Bing Xiao in Photonics and Nanoelectronic Labs. I have enjoyed working and talking with each of them, and I am thankful to have learned so much from them.

I would also like to acknowledge the Graduate Assistantships from the Department of Electrical and Computer Engineering, and Old Dominion University Research Foundation that were vital to the completion of this research.

Finally, I would like to thank my mother, brother for believing in me. I have special gratitude to my cousin Dr. Sufia and her family for their generous support during my stay in this University. I am also thankful to my friends, especially K. Ferdous for their support throughout this research.

TABLE OF CONTENTS

PAGE

LIST OF FIGURES

CHAPTER I

INTRODUCTION

1.1 AN OVERVIEW

Communication, computing, and information processing are moving toward higher bandwidth, higher speed, higher reliability, smaller size, lower power, and lower cost solutions. It seems that electronic devices can't satisfy all these requirements. Current electronics technologies have many obstacles, such as bandwidth problems, interference and vulnerability to non-local eavesdropping technique.

One possible solution to these obstacles is to convert some electronic devices to photonic devices. First, large bandwidth photonic devices have tremendous potential: since photons are not required to obey the Pauli's Exclusion Principle, all eigenstates of a photonic structure are always accessible to external photons. Furthermore, since photon-photon interactions are a second order effect and all other interactions are negligible, a photonic device provides a pristine environment for incoming photons, reducing heat generation and allowing outgoing photons to retain their original information in an unmolested form. Second, photonic devices are impervious to the usual non-local eavesdropping techniques. Signal interception from an optical component generally requires physical contact, so non-local methods are a priori ineffective.

At present, optical communication is a technological success story, and it is in search of all-optical network elements. The all-optical active and passive elements, some in the research,

some in the development phase, could satisfy most of the above requirements for communication. However, the progress of all-photonic signal processing and computing requires novel solutions. These solutions are already emerging. Undoubtedly; the 21st century will bring into this field the device applications of quantum effects, non-linear devices, metamaterials, and nanotechnology. All these areas overlap in photonic bandgap (PBG) structures [1].

1-D   2-D   3-D
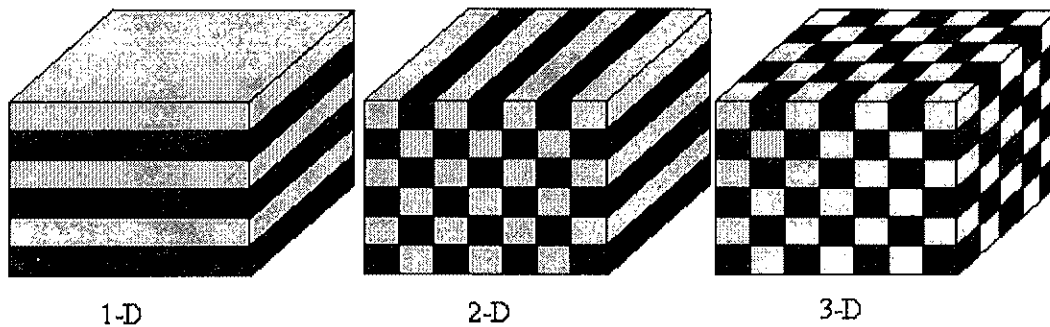
Figure 1. Schematic illustration of 1, 2, and 3-dimensional periodic dielectric structures.

Photonic crystal (PC) is a periodic dielectric structure, which can control the propagation of light passing trough it, analogous to semiconductors for electron. Depending on the dimension of periodicity it can be 1, 2 or 3 dimensional PBG structure (figure1). In semiconductors, the periodic potential for electrons in semiconductor leads to the formation of electronic band gap. In PBG materials, photons are constrained to propagate on energy bands and within a dielectric lattice. Photonic bands are the result of the multiple scattering of photons in the dielectric lattice. Unlike the natural periodic semiconductors, PBG materials are artificially produced and can be of unlimited forms, lead to the possibilities of producing many different novel devices. The study of electron in Semiconductor is governed

by Schrödinger's wave equation and quantum mechanics, is often diffracted by unwanted defects and has uncertainty features .On the other hand optical phenomena in a PC can be explained by Bloch theorem and Maxwell's equations are controllable and highly predictable. In photonic crystals, defects can lead to localized electromagnetic (EM) states, like its counter part in electronics; examples are high Q microcavities and linear wave guide in any media.

The history of the study of Electro magnetic waves in 1D periodic media began in 1887, when Lord Rayleigh first studied the multi-layer media. He identified a narrow band gap which hinders the propagation of light trough it. The gap changes with the incident angle and the periodicity of the materials. PBG materials are predicted theoretically as a means to localization and trapping of light in a bulk media over a band of frequencies [2, 3]. A direct corollary of this principle is the complete inhibition of spontaneous emission [4, 5], from an atom, molecule or electron hole pair excitation that is placed within PBG material. Indeed the emission frequency from atom lies within the PBG, the photon that would normally be emitted forms a bound state to the atom. Nearly all the novel phenomena of a PBG material are direct consequences of these effects. Thus, the introduction of 2D and 3D PBG after these discoveries completes the realization of the existence of a versatile PBG structure. Currently, the trend is up going and hundreds of research articles are published each year [6].

Current research on PC can be sub categorized in to calculation of PBG, fabrication, device application and quantum effects. PBG in a PC is produced by complicated interaction between macroscopic Bragg and microscopic Mie scattering. Hence, numerical analyses are

crucial to determine and design the properties of a PC. These techniques typically fall into three categories: the time domain methods, e.g. Finite Difference Time Domain (FDTD), which can model the time evolution of EM fields in these structures; the transfer matrix method (TMM), where scattering matrices are computed in order to obtain the transmission and reflection trough the structure; and frequency domain method, mainly, the plane wave expansion method (PWM) which proved very successful in searching the band gap in different geometries. However PWM has some s weaknesses, such as heavy computation and inability to deal with materials with dispersion and loss. Information obtained by TMM depends on many conditions of the numerical experiments, and may not be complete or accurate enough.

Following the development of theory, new designs and devices are proposed theoretically and fabricated experimentally. Due to the fabrication difficulty of 3D PBG structures, most novel devices are based on 2D PBG structures. Some of the important new devices are low loss sharp bend waveguide [8,11], high Q microcavity [11,13] , PBG planar antenna [14], microcavity defect laser with ultra low threshold current[18-21], high extraction efficiency LED [23], 100% channel add drop filter [24, 26], photonic crystal fiber [27] and so on .

Quantum effects in photonic crystals are of interest to many researchers. A few of those are control of spontaneous emission [3, 18, 28, 29], atom photon interaction in PBG environment [29, 31] and nonlinear effect in fiber or planar devices [33].

However, fabrication of such materials is not easy as calculation and design. Here lays the main bottleneck to develop a PC base system in commercial phase. Though several methods are proposed, few of them are good for large scale production. Many of those are inspired from current semiconductor fabrication techniques, as the principal choice of high dielectric constant materials are the same, e.g., Silicon, GaAs. Among them, silicon micro machining [34, 35], oval self organizing [36] and macroporous silicon[37-40] for 2D slab are more promising techniques.

1.2 PHOTONIC BAND GAPS

As stated before, in PBG materials, the formation of photonic band gap is a result of synergetic interplay between the macroscopic Bragg scattering and microscopic Mie scattering. Bragg scattering is related to the periodicity and geometry of the lattice; Mie scattering relates to the shape [41]. There exist complex relationships between these two scatterings with refractive index contrast. Hence there is no simple relation between the PBG structures and the bandgap. Numerical calculations become crucial to determine the optical properties of these structures.

No EM wave with the gap frequencies are allowed in the band gap. But when a disorder or defect is introduced, a localized state is created in the forbidden gap region. It allows the light of that particular range of frequencies to move around at that particular area. Hence "molding the flow of light" is possible.

1.3 SCOPE OF RESEARCH:

This work mainly focuses on silicon based 2D PBG structures. Photonic crystals fabricated with silicon have many advantages with respect to those fabricated with compound semiconductors: they can be built by using conventional microelectronics technology and are inherently CMOS compatible, show better optical properties due to the high refractive index difference between silicon and silica or air, and the starting materials are cheaper. However compound semiconductors have some advantages with respect to silicon. In particular they have better light emission properties and are easy to pattern with current microelectronics technology. The patterning process is a delicate step because it can lead to high surface recombination that can have a detrimental effect on device efficiency. The deep reactive ion etching (RIE) technique used to produce structures with a suitable depth leaves a non-negligible wall roughness that enhances losses by scattering. Self-assembly methods or macroporous silicon [37-40] formation methods are free from these drawbacks.

Active and passive modulation or tuning of band gap is crucially important to employ PCs in advanced technologies, e.g. for ultra-fast optical functions and all-optical switching. In recent years, several promising schemes for achieving this feature have been proposed. For example, tunability of the photonic band-gap (PBG) has been obtained by modulating the PC's refractive index through the electro-optic effect [42] or through temperature-induced changes in the PC's refractive index [43]. Chapter II is mainly focused on discussing the basics of 2 D photonic crystal, and current advancement in Si based PC devices, and band gap tuning. However, only a little variation is possible by dynamic tuning. So any post processing technique, causing wide change in band gap after fabrication, still provides a great deal of

flexibility in design and implementation of PC based devices. Oxidation and etching are quite mature techniques used in semiconductor industry for growing and removing SiO_2 layer on silicon. As a third dielectric layer, SiO_2 will change the band structure of the PC. Hence, the two methods may be used to modify the band structure of Si based PC. The goal of this thesis is to introduce these techniques and numerically observe the effect of introduced SiO_2 layer on the band structure of a Si based PC. Chapter III deals with the numerical procedure for modeling such effects. Chapter IV discusses the simulation results on different PBG structures. Chapter V demonstrates the application of oxidation and etching to tune the reference frequency of a single defect. Summary and conclusion of the research are drawn in Chapter V.

CHAPTER II

TWO-DIMENSIONAL PHOTONIC CRYSTALS

In the previous chapter a brief discussion is given on PBG structure and the preference of silicon as a PC material. Here, we will specifically deal with the fabrication techniques and the properties of a 2D PC. The first part is a comparison of the 2D PC with other dimensional structures and its optical properties without much mathematical interpretation. Then we will discuss previous work done on simulation and fabrication and on tuning the bandgap such structures. We will also highlight on structures based on macroporous silicon, as such structures are more suitable during fabrication.

2.1 ELECTRONIC BAND GAP VERSUS PHOTONIC BAND GAP

Photonic crystals usually consist of ordered or disordered arrays of dielectric scatterers, much like electronic crystals consist of ordered or disordered arrays of potential scatterers (atoms). For the case of the electronic crystal, variations in the potential serve as scattering centers for electrons. For the case of the photonic crystal, variations in the dielectric function serve as scattering centers for photons. In either case, one is able to construct an array of scattering centers, which serve as a diffraction grating. A simple model is then the Bragg diffraction [53] model, where the electrons or photons are scattered coherently by scattering centers whose periodicity is of the order of the particle wavelength. In fact, if the detailed pattern of the array of scattering centers is sufficiently complex, a highly nontrivial, frequency dependent, diffraction pattern will emerge. Depending on the specifications of the constructive and destructive interference inside the crystal, particles of a particular frequency will propagate

through the crystal with well defined group velocities. In very special situations, the destructive interference is complete and frequency regions where particles are unable to propagate, are created. These forbidden regions are known as band gap regions, and exist in both electronic and photonic crystals. More specifically, these band gap regions only sustain evanescent states i.e., states that exponentially decrease in real space, so that any incident particle (electron or photon) with a frequency within the band gap will be unable to propagate within the crystal lattice.

A useful way to quantitatively understand all of these effects is to solve the governing master equation for a specific electronic or photonic system.
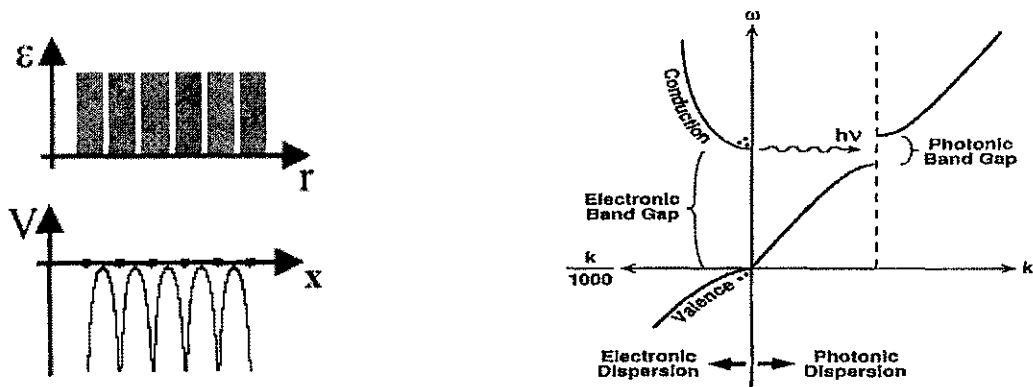
Figure 2. The modulation of the dielectric constant $\varepsilon(r)$ has the analogous effect, on photons, as the potential modulation $V(x)$ in a solid has on electrons. A comparison between dispersion relation or band structure is shown in the right hand figure. Right-hand side of the figure states the electromagnetic dispersion, with a forbidden gap at the wave vector of the periodicity. Left-hand side, the electron wave dispersion typical of a direct-gap semiconductor; the dots represent electrons and holes. After [7].

In both cases, the governing master equation is an eigenvalue equation that provides the allowable eigenvectors and eigenvalues of the system. For electronic system, it is derived

from Schrodinger's equation for an electron with effective mass m^* moving in a potential $V(x)$ varies randomly in space:

$$[\frac{-\hbar^2}{2m^*}\nabla^2 + V(x)]\psi(x) = \vec{E}\psi(x)$$ (2.1)

For a photonic periodic system the master equation are derived from Maxwell's equations:

$$\nabla \times \left(\frac{1}{\varepsilon(r)} \nabla \times \vec{H}(r) \right) = \left(\frac{\omega}{c} \right)^2 \vec{H}(r)$$ (2.2)

Here, the periodic dielectric function $\varepsilon(r)$ is analogous to $V(x)$, (see figure.2). Frequency (ω/c) is the eigen value and $\vec{H}$ is the eigen vector.

A photonic crystal can be classified into three categories based on the number of spatial dimensions where photon propagation is influenced: the periodic variation of dielectric function exists on those dimensions. (see figure 1). These are 1D, 2D and 3D PBG structures. According to their name, they have PBG properties only in certain number of dimensions where periodicity exists. For example, 3D PC has the complete PBG characteristics in all three dimensions.

2.2 REVIEWS ON 2D PHOTONIC CRYSTAL

2.2.1 Why 2D Photonic crystal?

1 D PBG structure obviously has intrinsic limitation of homogeneity in the plane and only periodic at one dimension; in addition the integration within an optical chip is not easy. On the other hand, 2D and 3D PC have better light confinement properties in terms of dimension and can be easily integrated within an optical chip.Although, the 3D structure has total light confinement in all three dimensions, the main difficulties to implement a 3D structure in different applications lie in its fabrication [44,45]. And it is almost impossible to implement any precise defect in a 3D structure with current technologies. However, in most applications two dimensional periodicity in light propagation is adequate if vertical confinement of light is possible by any other means. 2D Photonic crystal slab [46, 47] confines light in vertical z-direction by taking high aspect ratio (height versus diameter ratio of a hole or pillar in a 2D structure) and some index guiding mechanism, as in conventional in optical fiber. Thus, 2D PC becomes optimum choice for any real device application. Although in most theoretical calculation or in numerical modeling, 2D PC is considered as infinitely long in homogeneous dimension (i.e. z axis or vertical direction), a mere replication of the same results is possible for finite height slab structure with careful design [46].

2.2.2 Basics of Photonic Band Gap

Modulation of the dielectric constant periodically in the (x, y) plane forms the 2D photonic crystal. And homogeneity is maintained along the z direction. Different geometrical lattices can be produced: the most common ones are composed of air holes in a solid matrix, and solid pillars in air [48, 49]. Air can also be replaced by another dielectric material [50] at the

expense of a smaller dielectric index contrast. Generally, highest possible dielectric index contrast is desirable in order to open the widest photonic band gap.

In 2D PC, photon dispersion is strongly modified in the (x, y) plane with the appearance of photonic band gaps. In general, the photonic band gap opens for a particular polarization (TE or TM) and for a limited solid angle. In order to achieve an omni directional (e.g. a complete gap for one polarization), all the band gaps opened at different points of the Brillouin zone (BZ) have to overlap. The preferred lattice geometries to open a complete gap are the triangular and the honeycomb lattices [51]. The possibility of opening partial gaps for different polarizations allows the fabrication of polarization sensitive devices. The partial or complete character of the opened photonic band gap is defined, for a given lattice symmetry, by the relative volume of the different dielectric materials that compose the PC.

Photonic "gap map" or "bandmap" gives an overall picture of the existing band gaps at all direction in a PC for a TE, TM or both modes, as one or more of the parameters of the crystals are varied. In figure 3(a) such a map is drawn for triangular air hole lattice of silicon based 2D PC by varying the filling factor or r/a ratio (hole or pillar radius to pitch ratio).

A few rules of thumb can be drawn in order to optimize the material for maximum photonic band gap size and polarization [53- 55].

1. Connected higher dielectric lattice sites (e.g. veins) facilitate the opening of photonic band

gaps for TE modes, whereas isolated higher dielectric structures (e.g. pillars) are suitable for TM modes.

2. Triangular and honeycomb lattices can have complete photonic band gaps ,whereas a square geometry have only either TE or TM gap for hole or pillar type structure.

(a)   **(b)**
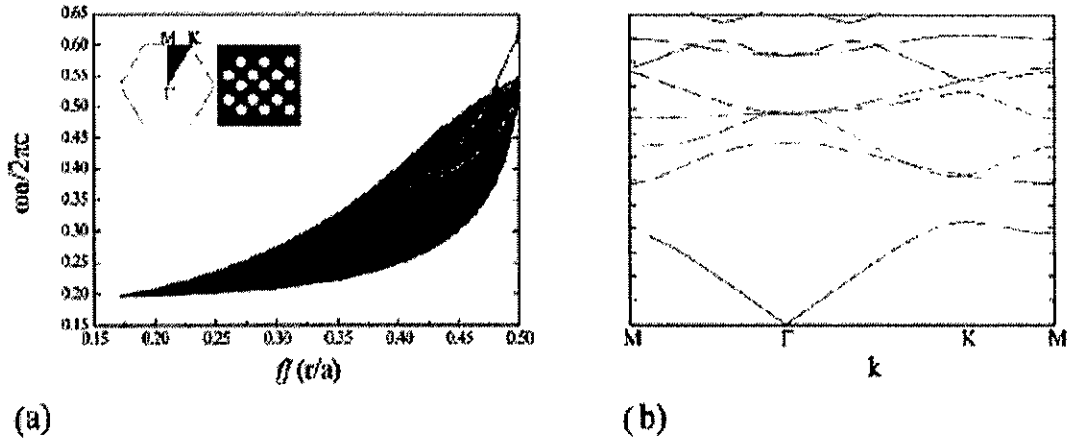
Figure. 3. (a) Photonic band gap map versus the filling factor ff = r/a. The *light gray* is the region where the TE band gap appears, the *black* indicates the region where band gaps open for TM modes, and the *hatched area* refers to the region where both TE and TM photonic band gaps exist. The *inset* shows the triangular lattice of holes in real space and in the reciprocal space with the main directions of the 2D Brillouin zone. (b) Band dispersion of a triangular lattice of holes (ε = 11.3) for a filling factor of 0.3.[53 have similar result for ε = 13].

3. If we define the *filling fraction* (ff) as the ratio between the pore radius (r) and the lattice pitch (a), then for a lattice of holes in a high-dielectric material the widest gap opens for ff $\leq$ 0.5, whereas for a lattice of pillars the best ff is at about 0.2 (more data can be found in [55]).

4. As for 1D, the frequency at mid-gap is defined by the lattice dimensions and, in particular, by the period. Moreover secondary gaps appear at multiples of this wave number.

5. Adding a small quantity of a third component enlarges the gap [56]. Higher dielectric constant is preferable.

Disorders in 2D PC play a fundamental role on the optical properties of the final structures. Introduction of defect actually helps to manipulate the light. In other word, defects make a PC useful for application like microcavities, wave guide and so on (see chapter I) .Like acceptor and donor states in its electronic counter part, defects create localized state of light in the forbidden gap region of a PC.

Nevertheless it is interesting to note that the opening of the fundamental photonic band gap is strictly related only to the periodicity of neighboring scatterer elements [57], while long-range disorder has no major influence. On the contrary, the secondary gaps are very sensitive to disorder in the lattice and disappear as the randomness increases. As an example, complete photonic band gaps were demonstrated in 12-fold quasi-crystal structures [58] even in materials with low dielectric constant.

Band calculations on PC are performed with similar methods as for electronic band calculations [59]. 2D systems have symmetry with respect to the plane of the system that enables us to decouple the TE and TM fields. This allows obtaining two different eigenvalue equations that can be solved independently. Plane wave expansion method (PWM) is the most preferred numerical technique to calculate the band dispersion of simple infinite perfect lattice [60-63]. In the PWM, the dielectric lattice and the related Bloch waves are approximated by a truncated Fourier series. Advantages of this method are its flexibility and simplicity that allow handling any geometry of the unit cell. For finite sized PC the PWM method can have convergence problems. In this case, real-space methods have to be used. These are based on a discretization of real space, in the time or in the frequency domains,

which allows us to solve the Maxwell's equations. PC with defects is difficult to simulate because the lattice symmetry is broken and no easy definition of the boundary conditions exists. For localized defects, such as a microcavity, a supercell method can be employed: defects are repeated periodically in the space where an effective lattice is formed with the unit cell containing the defect. If line defects are considered, either enormous supercells have to be computed or other approaches have to be used. One of the most frequently used is the finite difference time domain (FDTD) discretizing method to solve Maxwell's equations. Other information about band calculations can be found in [64] and references therein. A significant amount of work has been conducted in the Photonics Lab related to PWM and FDTD [30, 63].

Fabrication of 2D PC has been performed using different techniques [37-40, 64-66]. The most common utilizes a lithographic step to define the geometry of the lattice, followed by an etch step to form the vertical features that produce the modulation of ε in the plane. Depending on the material, either dry or wet etching has been used. Dry etching processes on III-V materials are well exploited and optimal results were obtained using the reactive ion etching RIE technique [67] or the chemical assisted ion beam etching CAIBE method [68].

2.2.3 Modulation of Band Gap Map

In order to modulate the band gap map of 2D PC we have to deal with certain parameters of the structure. In sec1.2 and 2.3 we mentioned that these parameters affect the multiple scattering and change the band gap. We summarize the parameters below, which affect the two scattering namely Bragg and Mie scattering,

- The type of symmetry of the structure or the lattice geometry.

- Dielectric constant contrast or refractive index contrast of the component materials.

- Filling factor, that is, the ratio between the volumes occupied by each dielectric with respect to the total volume of the composite.

- The topology, which can be either island: scattering centers are isolated from each other; or network: scattering centers are connected between them.

- The shape and size of the scattering centers.

A general discussion about topologies in PBG theory and the generalization to other classical waves can be found in [33].

Now, the modulation of the gap can be dynamic or static. To obtain a dynamic tunability in 2D PBG structure [70] several methods are used. Most of the tunability is performed by changing the refractive index contrast. It is done by inserting certain liquid material like polymer in the pore or void area of the PBG and tuning the resonance frequency electro optically [71, 72] or thermally [73]. Another way of changing the band gap on the fly is performed by deforming the lattice structure by applying mechanical stress [74, 75].

On the other hand, static modulation or post processing of the band gap of a 2D PBG is generally done by lithography; i.e., re-fabricate the device for new pitch (a) and/or pores or pillar radius [76].

Inserting a third dielectric or metal [77] will also change the band structure of 2D PBG.

2.3 SILICON BASED 2 D PHOTONIC CRYSTAL

The advantage of using silicon as a component of a 2D PC is already mentioned. Among

silicon we prefer macro porous silicon for its advantage to fabricate such structure. It has a

dielectric constant ε= 11.9, used in our calculation later. To fabricate such a structure, three

steps are followed [8, 38, 40]. First, the lattice geometry is defined by lithographic step. In

the   next   step,   an   alkaline   etching,   usually   by   KOH   is

(a)

(b)

(c)
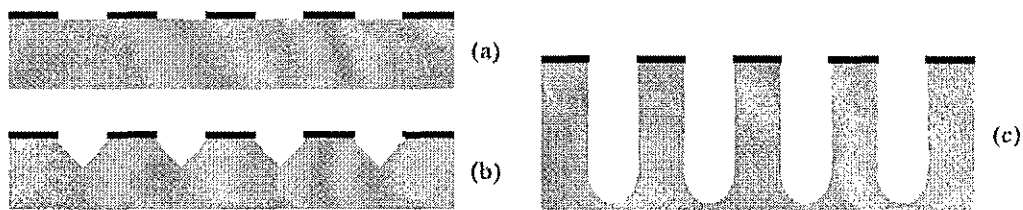
Figure. 4. Process steps needed in order to fabricate 2D PC on silicon by electrochemical etching: (a) Lattice definition; (b) alkaline etch pit formation; (c) electrochemical etching.

done in order to define the etch pit. In the final step, HF electrochemical etch step produces

vertical pores with smooth walls and high aspect ratio (see figure 4).

It is also important to distinguish between n and p type doped silicon in order to get high

aspect ratio macrospheres (see figure 5 and 6).
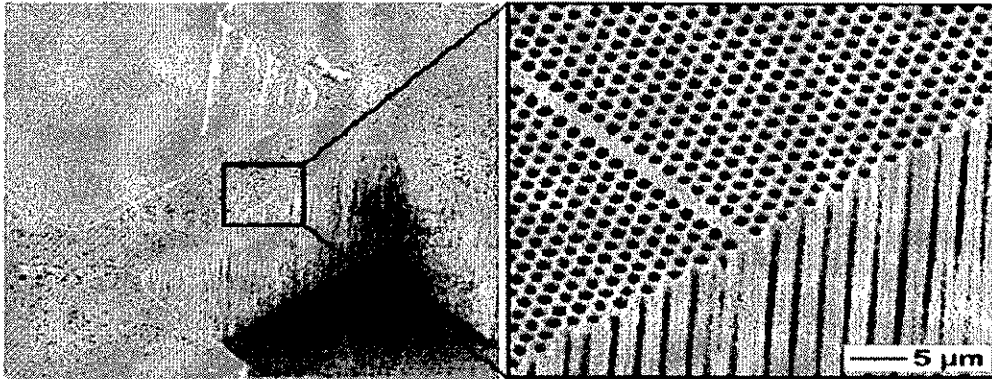
Figure 5. Photonic crystals produced on n-type silicon. After [40]
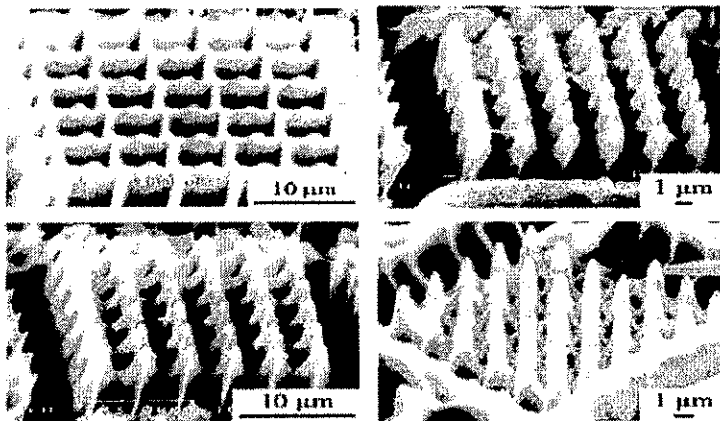
Figure 6. 2D PC formed on a p-type (20 Ω cm) Si substrate by macroporous silicon etching for different lattice constants. After [38].

To calculate a band structure, PWM is the preferred choice, which we have already mentioned. A triangular air hole lattice of Si 2D structure is mainly dominated by TE gap (see figure3 and 7). The fundamental band gap usually open near r/a=0.41 around a normalized frequency value of 0.4.
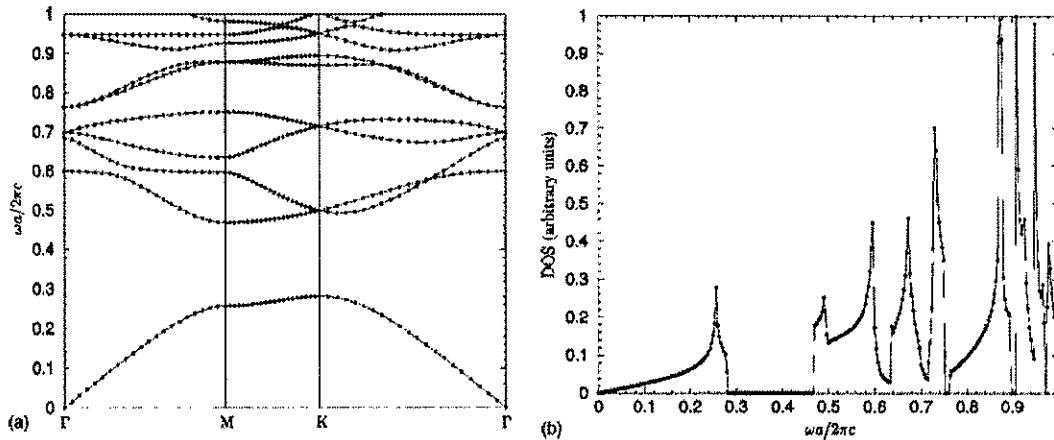
Figure 7. Two-dimensional band structure (a) TE mode and corresponding two-dimensional density of states (DOS) for a triangular lattice of air cylinders etched into macroporous silicon ($\varepsilon=11.9$). The filling ratio for air is 67% or r/a=0.43. After[36].

To measure photonic band structures experimentally, transmission or reflection is usually performed. A more direct method relies on resonant excitation of photonic modes by coupling of the $k_{\parallel}$ component of the incident light with a photonic mode in variable angle reflectance measurements. The excitation of a PC photonic mode produces a dispersive contribution in the reflectance spectrum. Recording the wavelength and knowing the incident angle the value of k is recovered by ($k_{\parallel}= \omega/c \; sin\theta$) (see figure 8). All the points ($k_{\parallel}$, ω) describe the dispersion band [12]. Not all the bands can be investigated in such experiment because of the broken mirror symmetry of the PC lattice at the surface of the sample.

Energy (eV)

Σ₃(E) T₃(E)
Σ₂(H) T₂(H)

a) odd TE

Σ₁(H) T₁(H)
Σ₄(E) T₄(E)

ω = ck

b) even TM

M Σ Γ T K M Σ Γ T K
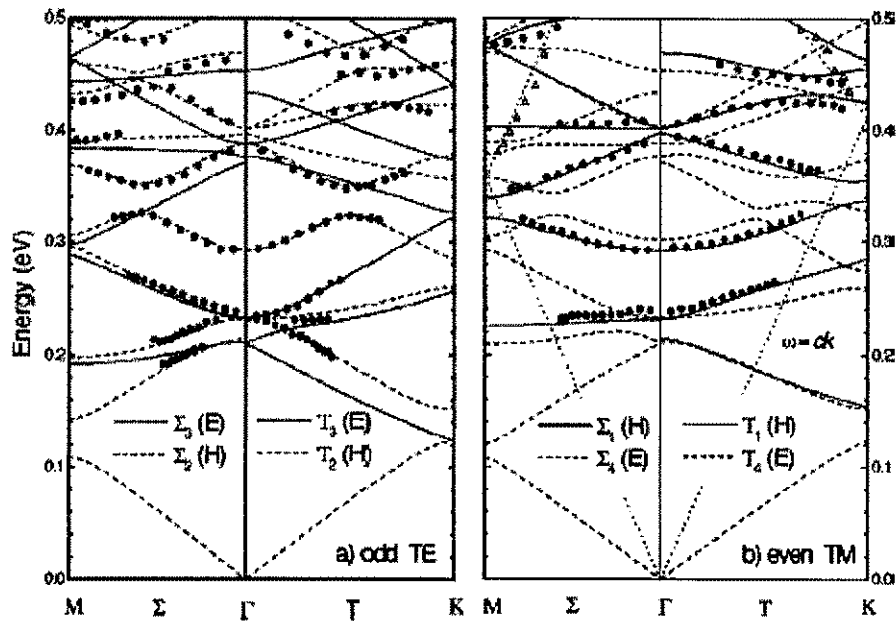
Figure 8. Points: measured dispersion of the photonic bands, derived from the structures in reflectance curves; solid and dashed lines: Photonic bands of the triangular lattice of air holes in Si with a=52 mm, r/a=50.24: , separated according to parity with respect to the plane of incidence: (a) TE polarization, odd modes, (b) TM polarization, even modes. The open triangles in (b) represent diffraction in air and must be compared with the folded dispersion of free photons (dotted lines). After [20].

In fact a detailed analysis of mode symmetry reveals that the only bands that can be probed by an external source are the ones with the same symmetry of the electromagnetic incident field. Many different experiments have to be used to analyze the complex phenomena related with photonic crystals. For example, large dispersive effects in PC can be analyzed by using phase-sensitive ultra short pulse interferometry.

2D PC offers the possibility to build small-volume, high-Q microcavity, easily integrable in optoelectronic devices with small dimensions (~20 μm).

When coupled with an active medium, the microscopic sizes of the cavity allow for ultra small lasers with very low power consumption and threshold-less operation [15]. In 2D, PC microcavities are composed by localized point-defects, obtained usually either by removing holes (pillars) or by modifying the dimension of one or more holes (pillars) in the PC lattice.

Passive photonic devices in silicon such as waveguides, couplers and splitters have been developed. Perhaps two important active devices are light emitters and modulators. Since silicon band gap is indirect, direct Si p-n junction emitters are highly inefficient. An alternative is the Raman silicon laser. Here a silicon photonic crystal wave guide is used to produce lasing effect in this optically pumped laser [21]. This source might find significant application in communication devices. Hence including other passive photonic devices will lead to photonic integration.

Intel has reported the first demonstration of the silicon modulator in the GHz range that is compatible with standard silicon CMOS fabrication process [17]. Again, this invention will lead to more integration of silicon photonic devices with CMOS. Since CMOS fabrication involves a myriad of processes, it is important to study the effect of processing on photonic devices. We choose oxidation and etching, the two fundamental processes to explore this topic.
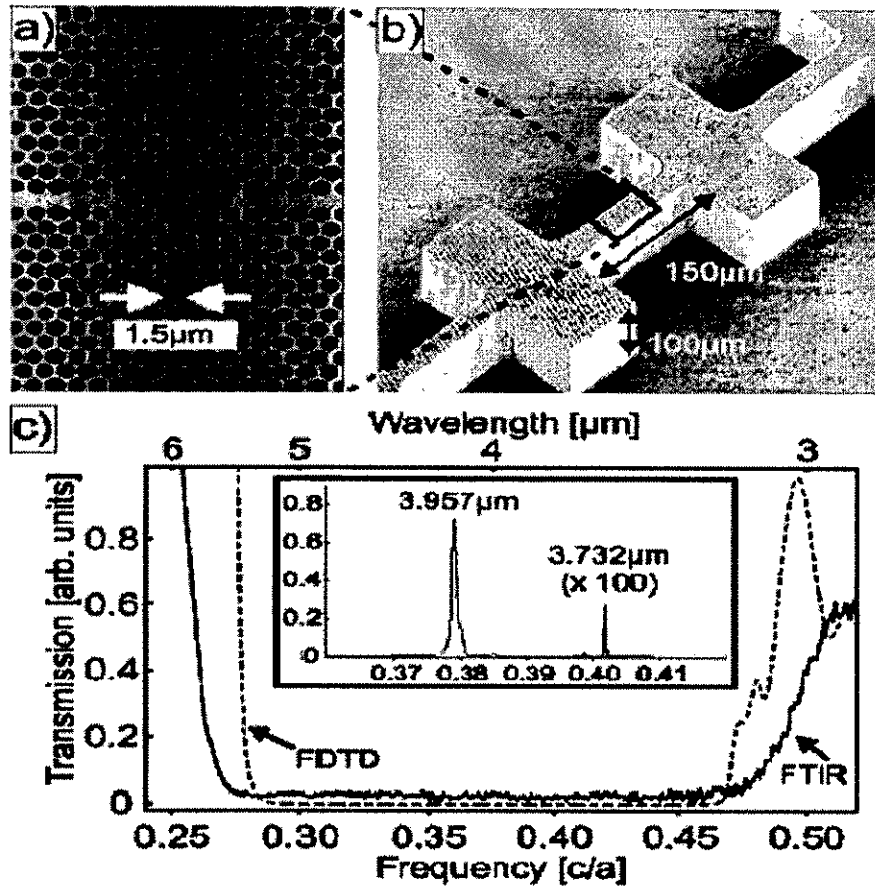
Figure 9. (a) Top view of a zoom into the region of the crystal containing the microresonator. (b) Overview of the photonic crystal substrate. (c) The *solid curve* shows the band gap spectrum of the structure in (b) measured by FTIR. The *dashed curve* displays the outcome of numerical simulations (FDTD) for a crystal without defects. When defects are introduced two resonances appear, as shown in the *insert*. After [15].

CHAPTER III

NUMERICAL ANALYSIS

Plane wave expansion method (PWM) is the most preferred numerical technique to calculate the band dispersion of simple infinite perfect lattice. It has become the de facto standard for computing the band structure of semiconductor-based photonic crystals [60-63]. In the PWM, the dielectric lattice and the related Bloch waves are approximated by a truncated Fourier series. Advantages of this method are its flexibility and simplicity that allow handling any geometry of the unit cell. For finite sized PC, the PWM method can have convergence problems. In this case, real-space methods have to be used. These are based on a discretization of real space, in the time or in the frequency domains, which allows us to solve the Maxwell equations. The research group at ODU Photonics Lab has developed suitable codes for PWM method [30, 63].

To begin with, we consider the propagation of a monochromatic electromagnetic field in a medium with a periodic distribution of the dielectric constant, $\varepsilon(r) = \varepsilon(r + \bar{R})$, with $\bar{R}$ a lattice vector. Then, the electromagnetic field distribution is governed by the master equation (2.2) or the wave equation. In a periodic medium, waves can be found propagating without scattering, and is equally true whether the waves consist of electrons or light beams.

In this chapter we will discuss a summary of Maxwell's equations and Bloch-Floquet theorem on propagation of EM wave through a periodic media. And then we will briefly

show the way to derive the necessary PWM equations to compute the band structure of a 2D PC.

3.1 MAXWELL'S EQUATIONS

The fundamental equations that form the foundation for electromagnetic theory are Maxwell's equations [22]. Written in differential form, these equations are,

$$
\left.
\begin{aligned}
\nabla \times \vec{E} &= -\frac{\partial \vec{B}}{\partial t} \\
\nabla \times \vec{H} &= \vec{J} + \frac{\partial \vec{D}}{\partial t} \\
\nabla \bullet \vec{D} &= \rho \\
\nabla \bullet \vec{B} &= 0
\end{aligned}
\right\}
\qquad 3.1
$$

where E is the electric field intensity, B is the magnetic flux density, H is the magnetic field intensity, and D is the electric flux density. The electric current density J and electric charge density ρ are the sources of the electromagnetic fields.

For linear and isotropic media, $\vec{E}$ and $\vec{D}$, and $\vec{B}$ and $\vec{H}$ are related by the constitutive relations,

$$
\left.
\begin{aligned}
\vec{D} &= \varepsilon_r \varepsilon_0 \vec{E} \\
\vec{B} &= \varepsilon_r \varepsilon_0 \vec{H}
\end{aligned}
\right\}
\qquad 3.2
$$

Here ε_0, μ_0, ε_r, and μ_r are the free-space permittivity, free-space permeability, relative permittivity, and relative permeability, respectively. Note that dielectric constant of a media $\varepsilon = \varepsilon_0 \cdot \varepsilon_r$.

Now we will consider electromagnetic waves in materials with

- source free space: $\rho(r) = 0$, $\vec{J}(r) = 0$.

- Lossless medium: $\varepsilon(r)$ is real in the interested region.

- Linear and time invariant, so that we can use the plane wave theory or Fourier theory.

- Non magnetic material: $\mu_r = 1$.

Using complex value expression for equation (3.1) and (3.2) we can derive the master equation for a photonic periodic structure similar as equation (2.2):

$$\nabla \times \left(\frac{1}{\varepsilon(r)} \nabla \times \vec{H}(r) \right) = \left(\frac{\omega}{c} \right)^2 \vec{H}(r)$$

(3.3)

This master equation along with

$$\nabla \bullet \vec{H}(r) = \nabla \bullet \vec{D}(r) = 0$$

(3.4)

completely determines the $\vec{H}(r)$.

So for a given photonic crystal $\varepsilon(r)$, solving the master equation can give us $\vec{H}(r)$. And from there we can determine $\vec{E}(r)$ from Maxwell's equation. We use the equation for $\vec{H}$ instead of $\vec{E}$ or $\vec{D}$ since the operators for $\vec{E}$ or $\vec{D}$ are not Hermitian and do not posses some of the properties of a Hermitian discussed later in this section. By inspection, we can verify that equation 3.3 is a Sturm-Liouville eigenvalue problem [25], same as the Schrödinger's equation. One important difference however, is that unlike their electronic counterpart, photonic crystals have no fundamental length scale like Bohr radius: they are scale invariant. This means that a linear scaling of the coordinates describing the dielectric function results in

nothing more than a linear scaling of the eigenvalues. For example, changing the mode profile by changing the length scale by a factor 's', needs only to scale the old mode and its frequency by the same factor. Hence the solution of a problem at one length scale provides the solutions at the other length scale. Later in chapter IV, we use gap-midgap ratio, a ratio of band gap width to its midgap frequency, to characterize a photonic crystal with a particular geometry, rather than only by gap width or midgap frequency; because this ratio is free from any length scale of the crystal, it is free from the scaling properties of the master equation.

There are a few more mentionable properties of the master equation. The operator $\Xi = \nabla \times \frac{1}{\varepsilon} \nabla \times$ in equation (3.3) is a linear hermitian operator; if $\vec{H}_1$ and $\vec{H}_2$ are two different modes then $\vec{H}_1 + \vec{H}_2$ is also a mode and $(\vec{H}_1, \Xi \vec{H}_2) = (\Xi \vec{H}_1, \vec{H}_2)$. The operator must have real eigenvalues only if the dielectric function is positive everywhere. Any two different modes are orthogonal, i.e., $<\vec{H}_i, \vec{H}_j> = \delta_{ij}$. Degenerate modes are not necessarily orthogonal.

3.2 PROPAGATION OF WAVE IN PERIODIC MEDIA

If we extend our propagation of wave trough a periodic media, we have to apply Bloch-Floquet's theorem. One of the many interesting problems in mathematical physics is the solution of the wave equation in periodic media. The solution of this type of equation is usually derived using a form of Floquet's theorem, determines a particular periodic solution of Mathieu's equation, the equation of wave motion. It provides the basis of quantum band theory. Band theory, which describes the properties of electrons in a periodic potential due to

the atomic arrangement of atoms in a crystal, is the foundation for the understanding of electronic transport in metals, semiconductors, and insulators. The solution of the periodic potential problem can be expressed in mathematical form as Bloch's theorem. Bloch's theorem states that the eigen functions of the Schrödinger's equation for a periodic potential are the product of a plane wave and a function which has the same period as the periodic potential. A number of similarities can be seen in the solution of electron wave propagation in semiconductors and electromagnetic wave propagation in periodic dielectric media, and Bloch's theorem can be extended to electromagnetic wave propagation in periodic media. According to the theorem, waves in a periodic medium can propagate without scattering.

3.3 PLANE WAVE EXPANSION FORMULATION

To derive the photonic band structure, we construct the real space lattice vectors that describe the periodicity of the dielectric function. We then construct the corresponding set of reciprocal lattice vectors $\vec{G}$, and expand the inverse dielectric function in a Fourier series on the reciprocal lattice:

$$\varepsilon(r) = \sum_{\vec{G}} \varepsilon(G) e^{i\vec{G} \cdot \vec{r}}$$

(3.5)

Since our dielectric function $(\varepsilon(r))$ and its Fourier expansion coefficient $(\varepsilon(G))$ are periodic with discrete translational symmetry, it can be expressed as,

$$\varepsilon(G) = \frac{1}{V} \oiiint_{\Omega} \varepsilon(r) e^{i\vec{G} \cdot \vec{r}} d\Omega$$

(3.6)

Where, Ω is the unit cell and V is the volume of unit cell. We apply Bloch's theorem and require the solutions to the master equation (3.3) to have the form and expand it for a mode in a periodic structure as a sum of infinite number of plane waves,

$$\vec{H}(r) = e^{i\vec{k}\bullet\vec{r}}h(r)\hat{e}_k$$

(3.7)

$$= \hat{e}_k e^{i\vec{k}\bullet\vec{r}}\sum_{\vec{G}}h(G)e^{iG_i\bullet\vec{r}}$$

$$= \sum_{\vec{G},\lambda}h(G,\lambda)e^{i\vec{G}\bullet\vec{r}}\hat{e}_\lambda$$

(3.8)

where, $\lambda = 1,2$; $\vec{k}$ is the wave vector of the plane wave, $\hat{e}_\lambda$ represents the two unit axis perpendicular to the propagation direction $(\vec{k}+\vec{G})$, i.e., $\hat{e}_1,\hat{e}_2$ and $(\vec{k}+\vec{G})$ are perpendicular to each other. $h(G,\lambda)$, is coefficient of H components along the axes $\hat{e}_\lambda$. In equation (3.8), the transverse property is used to decompose the wave into sum of a set of plane waves, which is the main idea of the PWM.

Finally, Helmholtz equation can be transformed to an algebraic form [30],

$$\sum_{G'}\left|\vec{k}+\vec{G}\right|\left|\vec{k}+\vec{G}'\right|\varepsilon^{-1}(\vec{G}-\vec{G}')\begin{bmatrix}\hat{e}_2\cdot\hat{e}_2' & -\hat{e}_2\cdot\hat{e}_1' \\ -\hat{e}_1\cdot\hat{e}_2' & \hat{e}_1\cdot\hat{e}_1'\end{bmatrix}\begin{bmatrix}h_{1,G'} \\ h_{2,G'}\end{bmatrix} = \frac{\omega^2}{c^2}\begin{bmatrix}h_{1,G} \\ h_{2,G}\end{bmatrix}$$

(3.9)

This is a standard eigen value problem and can be solved numerically. In this thesis, we are only interested in the periodic propagation of plane wave in 2D photonic band structure. Hence, we only concentrate on the (x,y) plane propagation of the EM wave. As $\vec{k}$ and $\vec{G}$ are

in the same (x,y) plane, $(\vec{k}+\vec{G})$ is also in (x,y) plane. It leads to $\hat{e}_1 = <\cos\theta, \sin\theta, 0>, \hat{e}_2 = <0,0,1>$, then:

$$\begin{bmatrix} \hat{e}_2\hat{e}_2' & -\hat{e}_2\hat{e}_1' \\ -\hat{e}_1\hat{e}_2' & \hat{e}_1\hat{e}_1' \end{bmatrix} = \begin{bmatrix} 1 & 0 \\ 0 & \cos(\theta-\theta') \end{bmatrix} \tag{3.10}$$

i.e, the $2N \times 2N$ matrix equation can be decoupled into TE and TM mode equation. Using equation(3.10), from eq (3.11) we can get the independent relation for the TE and TM waves respectively,

TE: $$\sum_{G'}(\vec{k}+\vec{G}) \bullet (\vec{k}+\vec{G}')\varepsilon^{-1}(\vec{G}-\vec{G}')h_2(\vec{G}') = \frac{\omega^2}{c^2}h_2(\vec{G}) \tag{3.11}$$

TM: $$\sum_{G'}|\vec{k}+\vec{G}||\vec{k}+\vec{G}'|\,\varepsilon^{-1}(\vec{G}-\vec{G}')h_1(\vec{G}') = \frac{\omega^2}{c^2}h_1(\vec{G}) \tag{3.12}$$

3.4 IMPLEMENTATION

Our modeling of Si based 2D PBG is limited to circular cylindrical hole or pillar structure, which is defined as 'atom'. For simplicity, we assume the number of 'atoms' in the unit cell or supercell is finite. The first step is to determine the unit cell or supercell; then it is easy to calculate the set of reciprocal lattice vector $\vec{G}$ (r) and unit vectors $\hat{e}_1, \hat{e}_2$. The key part is to obtain the Fourier coefficient matrix $\varepsilon(\vec{G}-\vec{G}')$ according to equation (3.6). In order to obtain this, one have to calculate the Fourier coefficient of a single atom first using analytical or numerical Fourier transform, and then calculating the Fourier coefficients for the supercell using shift property. Finally we rearrange to get the coefficients $\varepsilon(\vec{G}-\vec{G}')$ and then by inversing get $\varepsilon^{-1}(\vec{G}-\vec{G}')$.

Analytical Fourier transform is more preferable to its numerical form, in terms of modeling accuracy and programming complexity, when it is available. Figure 10 gives the schematic of a unit cell of possible structure for this modeling. We already mentioned that in this case SiO_2 is our third dielectric material. The inner radius of the cylinder is r_a; the outer radius r_c is the combination of r_a and the third dielectric layer thickness x_0. The dielectric constant for the atom, background and the third dielectric material are ε_a, ε_b and ε_c respectively.
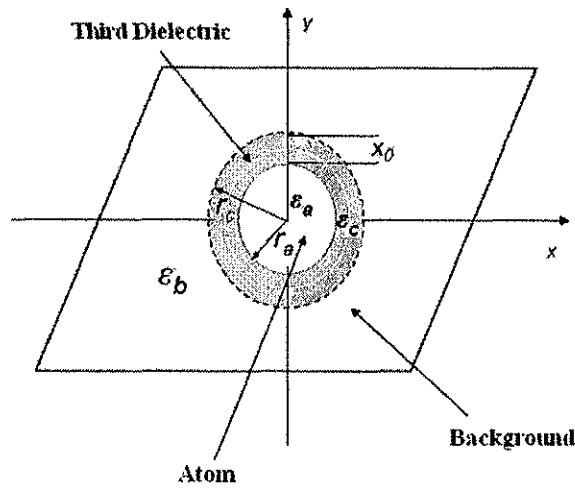
Figure 10. Schematic of an unit cell of a possible PBG structure. Here, r_a is the radius of the hole or pillar known as atom. x_0 is the thickness of the third dielectric layer, in this case SiO_2. r_c is the combination of r_a and x_0. The white circle indicates the initial radius of the atom when $x_0=0$, i.e. r_c $=r_a$. ε_a, ε_b and ε_c are the die-electric constant of the indicated materials.

The lattice structure can be represented by the two lattice basis vector $\vec{a}_1$ and $\vec{a}_2$. The area of the unit cell is calculated as $A = | \vec{a}_1 \times \vec{a}_2 |$, the Fourier transform of the unit cell is

$$\varepsilon(G) = \varepsilon_b \delta(|\vec{G}|) + 2(\varepsilon_c - \varepsilon_b) f_c \frac{J_1(|\vec{G}|r_c)}{|\vec{G}|r_c} + 2(\varepsilon_a - \varepsilon_c) f_a \frac{J_1(|\vec{G}|r_a)}{|\vec{G}|r_a}, \quad (3.13)$$

where J_1 is the 1st order Bessel function and $f_{cylinder}$ (cylinders corresponding to r_a and r_c, f_a or f_c) is a fraction parameter: $f = {Vol_{cylinder}}\big/{Vol_{cell}}$. For a different lattice structure only the values of f and G vary, the Fourier transform remains the same as equation(3.13).

When there is no third dielectric layer the eq (3.13) becomes equation(5) in ref [63].

Here is a summary of the steps to determine the band structure of a PC using PWM.

1. Given a k point to solve the associating frequency ω.

2. Find the reciprocal lattice and choose the reciprocal vector $\vec{G}$ set.

3. Find each of the Fourier transform coefficient $\varepsilon^{-1}(\vec{G} - \vec{G}')$.

4. Find $(\vec{k} + \vec{G})$ and two unit vector sets.

5. Form the corresponding eigen value problem matrix following equation(3.11) and (3.12).

6. Calculate the eigenvalues.

From the calculated eigen value we can plot the k-ω relationship or the band structure. In the periodic structure, according to Bloch's theorem the relation ship is also periodic, so it is enough to calculate k points in the first Brillouin zone or irreducible Brillouin zone.

The thickness of SiO_2 layer, x_0 is dependent on the both atom and background volume. It varies with the silicon as atom or background materials and whether it is oxidation or etching. Hence, the dimensions of silicon and air layer are also varied accordingly. A more details explanation can be found in Appendix I.

3.5 DEFECT MODE CALCULATION

We modeled a single defect cavity in a 2D square lattice of silicon pillar as 2D PC. We use

software based on FDTD method to solve this defect mode. Detailed description of this work

and procedure can be found in [30]. We determine the shift in frequency after altering the

defect by oxidation and then partial or complete etching of the oxide.

CHAPTER IV

RESULTS AND DISCUSSION

In this chapter we discuss the result of our modeling. The main objective of this thesis is to observe the effect of SiO_2 layer insertion in a Si based 2D PC, infinitely long in homogeneous vertical direction. SiO_2 can be grown by oxidation and then layer thickness can be reduced by etching on Si surface. To observe the propagation of EM wave in periodic structure, we are only interested on SiO_2 grown perpendicular to the plane of propagation, i.e., along the hole or pillar.

Insertion of SiO_2 layer will change the band structure of the PC. Band map is a convenient way to monitor the change in band gap in any band structure compositely. Another measurement of a PC performance is gap-midgap ratio (ratio of band gap width to the mid gap frequency). These are also discussed more elaborately in previous two chapters.
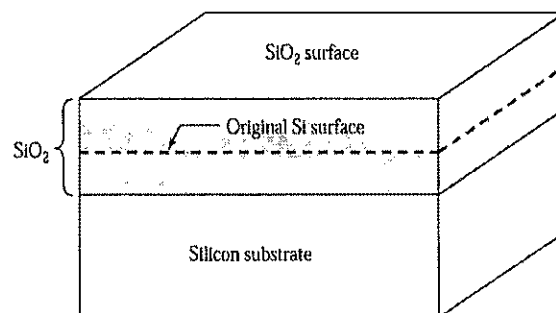
Figure 11. SiO_2 growth by thermal oxidation. Silicon is consumed.

We model the both TE and TM band map after oxidation and etching for a particular initial r/a (hole/pillar radius and pitch ratio) by altering the thickness of the SiO_2 layer.(See Appendix-I).Note that, every dimension of a PC is normalized with its pitch.

Square and triangular lattice structure for both air hole and Si pillar type configuration is covered. Among these lattice structures only triangular lattice air hole structure has significant complete band gap and has more practical interest in terms of device designing. For that reason, we choose this as our principal structure to observe the band gap change and discuss it more extensively. In any structure, fundamental band gap for each mode is usually significant in size and principal interest. Hence, in our discussion unless otherwise stated, 'band gap' or any thing related to that usually refers the fundamental gap for that particular lattice structure for any mode. General discussions about the lattice structures and configurations and typical shape of their band gap maps plotted against r/a can be found in [53].

4.1 SILICON PHOTONIC CRYSTAL - TRIANGULAR LATTICE OF AIR HOLES

This PBG structure has triangular air hole geometry on a Si substrate and it has a hexagonal Brillouin zone(BZ) (figure 12a). We use r_0 to specify the initial radius of the air column when there is no SiO_2 layer in the structure.

Figure 12(b) shows a typical band map for our PC with $\varepsilon=11.9$, as the value of r/a is varied; for higher r/a ratio, a large fundamental TE band gap dominates the map. The vertical line on r/a axis in figure 12(b) indicates the maximum Complete Band Gap (CBG) 16.2% at $r/a=0.477$. (Same as [36].)

(a)   (b)
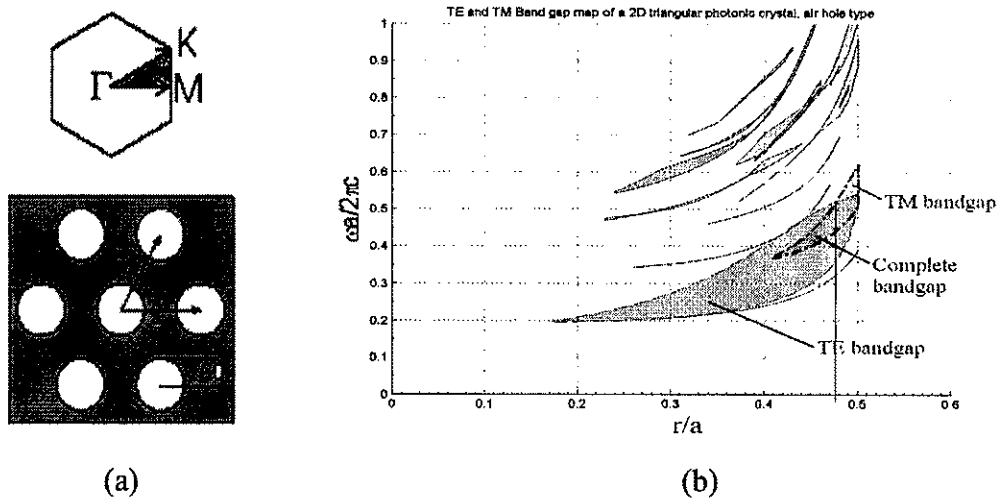
Figure 12. (a)Schematic and Brilloin zone and (b) gap map of a Si air column triangular lattice PC. In (a), r is the radius of the air column with the initial value r_0, and a is the pitch (center to center hole spacing) of the PC. Shaded area in BZ indicates the irreducible Brillouin zone (IBZ) In (b) , the vertical line at $r/a=0.477$ indicates the largest CBG.

4.1.1 Effect of Oxidation

Now let us oxidize the structure. We can grow a SiO_2 layer inside the holes, leading to a new

dielectric oxide layer between silicon and air making the PC a $Si/SiO_2/air$ composite material.

Oxidation will also change the dielectric constant contrast and the inner dimensions of

corresponding unit cell of the PC, while keeping the pitch a constant. The resulting structure

is depicted in the figure 13.

(a)   (b)
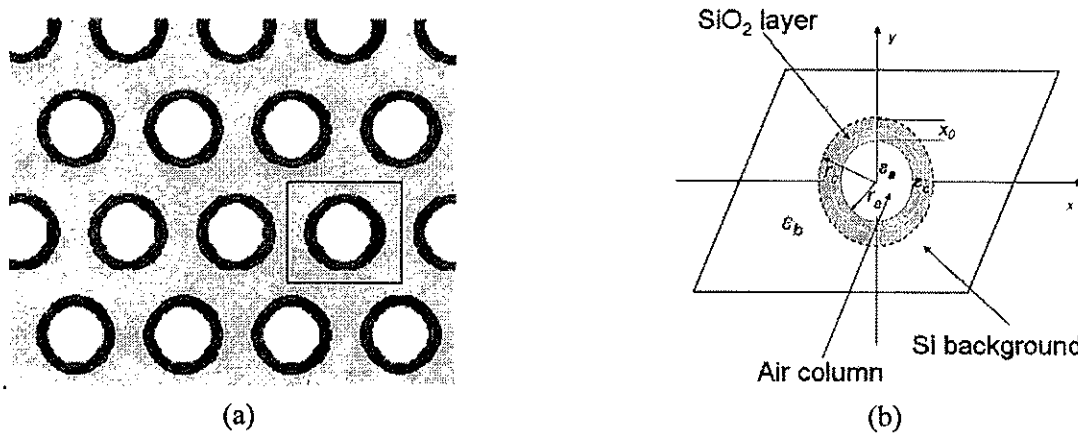
Figure.13. Schematic of the structure resulting from oxidation of the silicon PC. (a) is the portion of a
bulk crystal and (b) is the enlarged details of an air column and its vicinity marked inside the square
in (a). r_a is the current radius of air column and $x0$ is the thickness of the SiO_2 layer. r_c is the
combination radius of air and SiO_2 column. The white circle in SiO_2 layer area indicates the initial air
column radius (r_0) when there was no SiO_2 layer. ε_a, ε_b and ε_c is the Die-electric Constant of the
indicated materials. $r_c = r_a + x_0$.

At first we calculate the band gap for $r_0/a=0.46$ with filling ratio of 33% Si. Then we

increase the normalized thickness of the SiO_2 layer (x_0/a) by oxidation and calculate the band

gap again. The results are shown in figure 14. Both TE and TM mid gap frequencies increase

with oxidation. While TM gap width increases, TE gap width decreases with the increase of

x_0/a. Thus the TE gap-midgap ratio decreases from 45% to 35% for the fundamental gap (See

figure 15). On the other hand, corresponding overlapping TM gap to midgap ratio keeps

increasing from 12% at x_0/a =0, attains its maximum value of 13.46% at x_0/a =0.06 and decreases 13.34% at $x0/a$ = 0.07. (figure 15) The second and third TM band gaps are also wider at higher frequency and higher x_0/a.
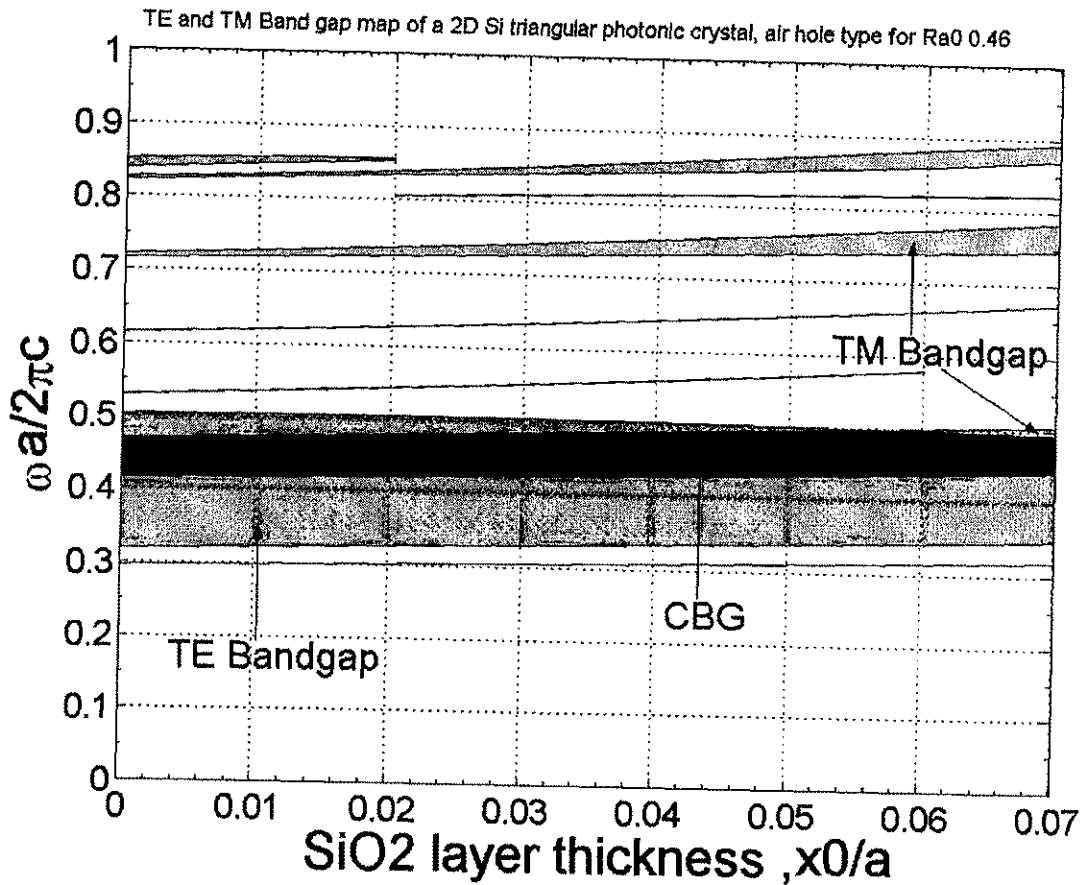
Figure 14. Gap map of the triangular air hole 2D Si PC with increasing SiO_2 layer due to oxidation. Here r_0/a= 0.46.
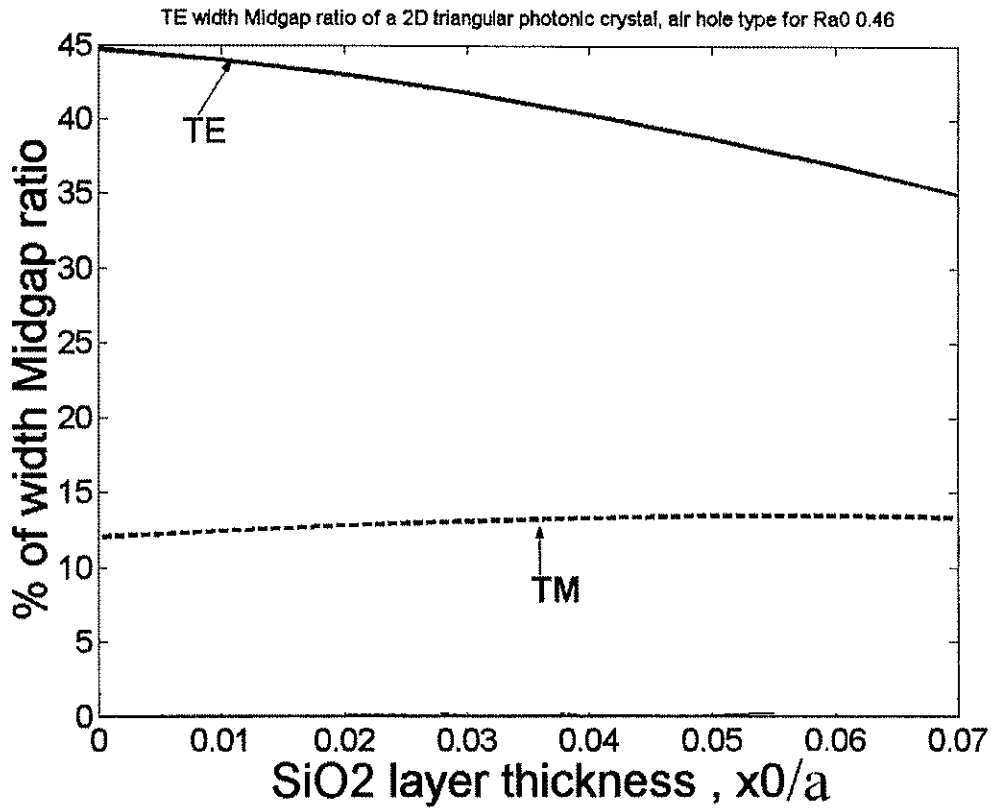
Figure.15 Gap- midgap ratio of the fundamental TE and TM mode band gap with increasing SiO_2 layer due to oxidation. Here r_0/a=0.46.

The CBG produced by the overlap of TE and TM band gaps increases due to mainly the increase of TM band gap as long as it completely overlaps the TE band gap. But at higher thickness of SiO_2 layer, TM and TE band gap start to move apart from each other and overlap only partially. As a result, CBG decreases more rapidly at higher thickness. Figure 4.5 shows the complete band gap-mid gap ratio for various r_0/a. As an example, for r_0/a= 0.46, the ratio is nearly 12% when there is no SiO_2 layer and becomes maximum (13.44%) at x_0/a= 0.05. At this point TM band gap starts to move away from TE band gap and the ratio decreases to 11.06% at x_0/a=0.07.
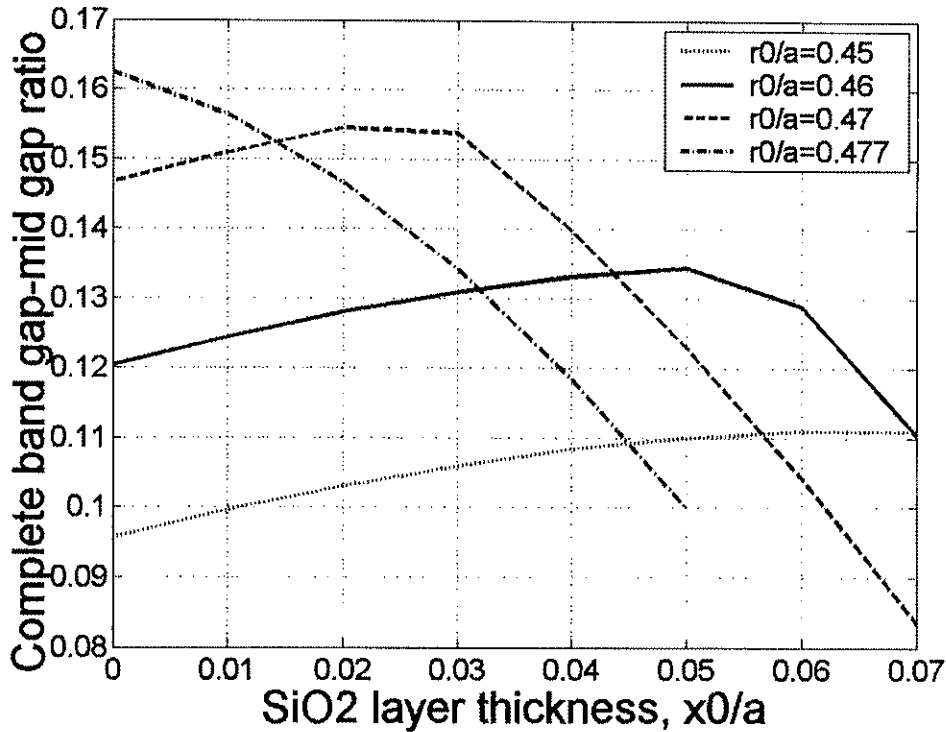
Figure 16. Complete band gap-midgap ratio of a Si PC for different r_0/a for varying SiO_2 layer thickness x_0/a, due to oxidation.

For other values of r_0/a, CBG decreases, due to the same reason, at a particular thickness of SiO_2 layer. At $r_0/a=0.477$, for which the maximum CBG is usually achieved for a PC of regular silicon triangular lattice, the CBG decreases with the increment of SiO_2 layer. In any case, CBG of a Si PC with SiO_2 is not greater than its maximum value of 16.2% of a regular one. It is important to note that the maximum thickness of SiO_2 that can be grown is such that the combined diameter of air column and SiO_2 does not exceed the pitch value a. At this stage, all the silicon material is converted into silicon dioxide.

4.1.2 Effect of SiO_2 Etching

Silicon dioxide can be selectively etched in hydrofluoric acid without affecting silicon. Thus the partial or complete etching of SiO_2 changes the band map in an irreversible way (figure

17). Etching decreases the thickness of the SiO$_2$ layer thereby increasing only the air column radius, while maintaining the dimension of Si the same as it was at the end point of oxidation. During the etching process, the TE band gap decreases while that of TM increases. Similarly, the TE gap-midgap ratio decreases while that of TM increases with SiO$_2$ etching. The change is opposite of what we observed during oxidation, but with a steeper slope. Since CBG depends on the overlap of TM and TE band gaps, it is found to increase with decrease in SiO$_2$ due to etching. Thus the effect of etching on CBG is significantly different from oxidation, as can be seen by comparing figure 14 and figure 17.
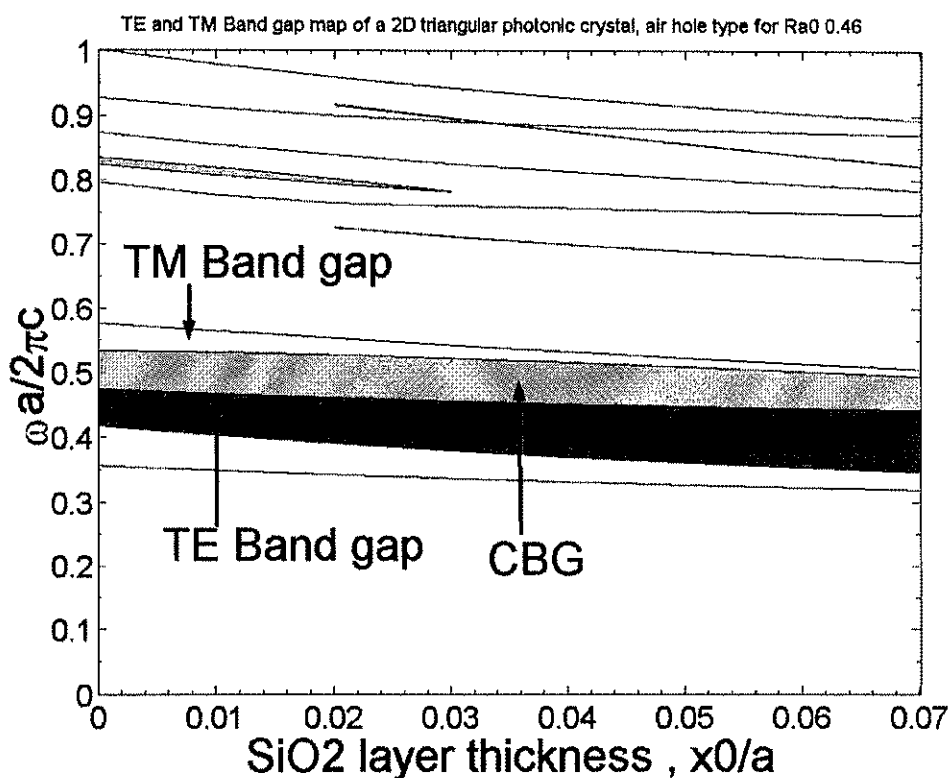
Figure 17. Band map and gap-midgap ratio triangular Si PC (r_0/a=0.46) with decreasing SiO$_2$ layer after etching, began at the SiO$_2$ layer thickness x_0/a =0.07.
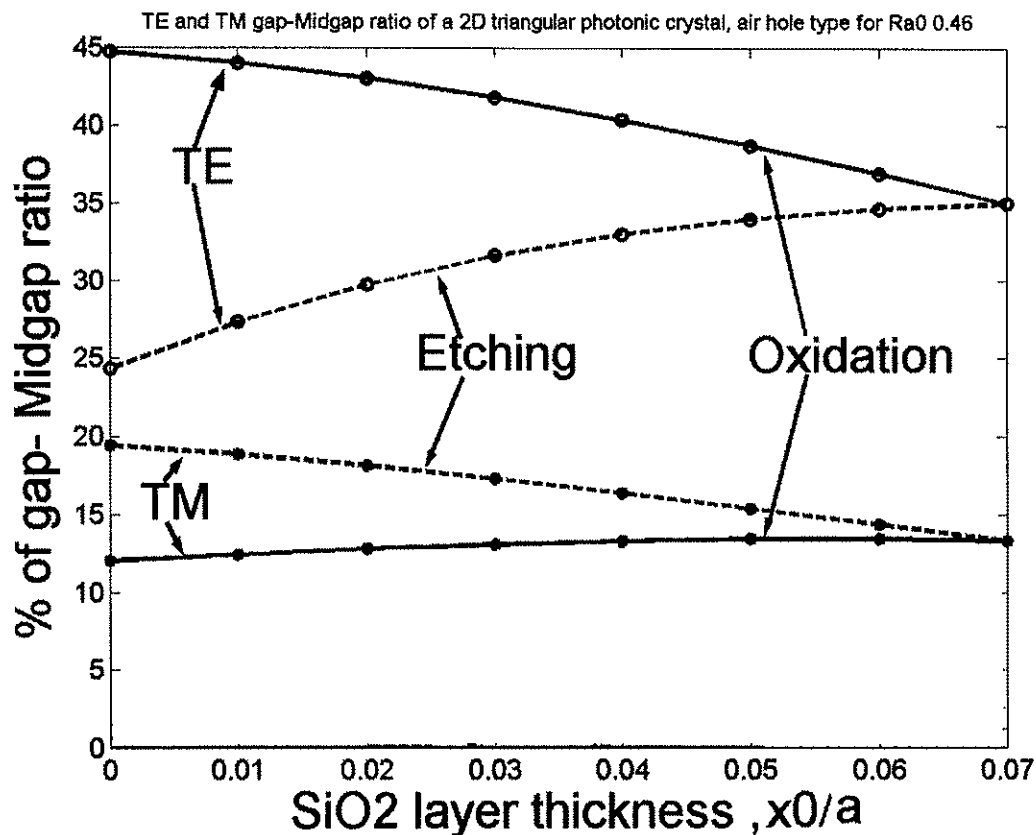
Figure 18. TE and TM gap-midgap ratio triangular air hole 2D PC (r_0/a=0.46) with decreasing SiO$_2$ layer after etching, compared with oxidation, began at the SiO$_2$ layer thickness x_0/a =0.07.

Hence, by varying the thickness of SiO$_2$ layer by oxidation and/or etching, it is possible to tune gap width and mid gap frequency for a particular r_0/a. The gap-midgap ratio is particularly interesting so as to observe the effect of oxidation and then etching partially or completely at different thickness of SiO$_2$ layer. For the case of r_0/a=0.46. Figure 17 shows the fundamental complete gap-mid gap ratios obtained by growing SiO$_2$ layer by means of oxidation (solid line). The dotted lines show the effect of etching SiO$_2$ at various points after oxidation.
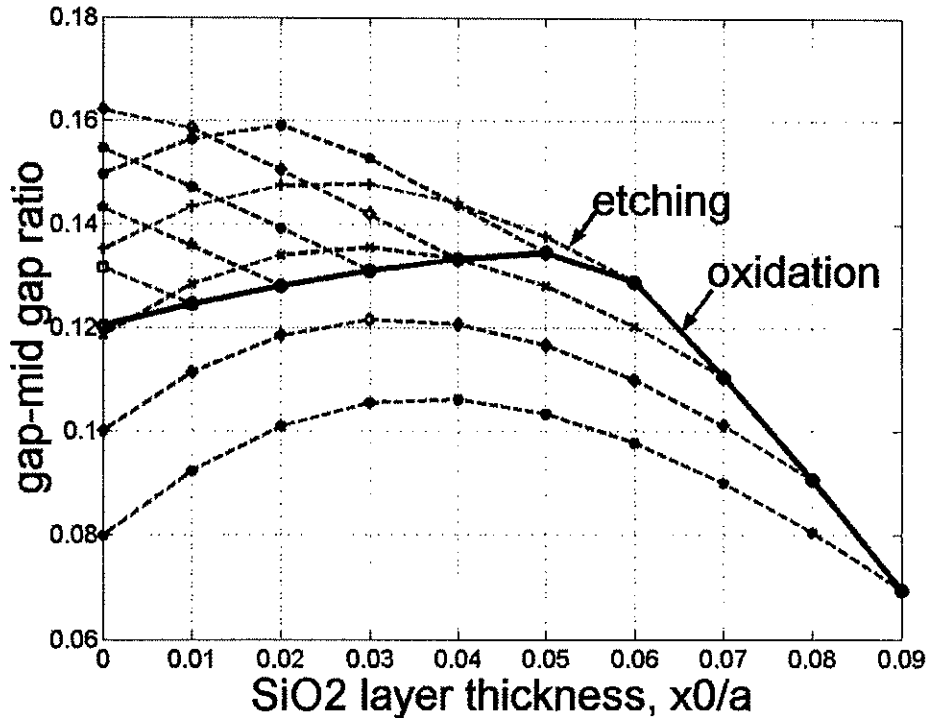
Figure 19. Complete gap-midgap ratio of a triangular Si PC with varying SiO_2 layer thickness, by oxidation and etching, at r_0/a=0.46. Solid line indicates the gap-mid gap ratio due to oxidation. The dotted lines are for etching that starts from different points on the solid line.

For complete etching carried out before the ratio reaches maximum, the ratio can be increased further. On the other hand, if the etching is done at a higher oxide thickness where the ratio has surpassed the maximum, after etching the ratio is found to be lower than that for r_0/a=0.46. This effect is due to the changes in the silicon-filling ratio. The processes do not change the lattice spacing, a. In any case, our results show that it is possible to obtain a wide range of gap widths and mid gap frequencies at fundamental frequency using oxidation and etching. The processes introduce gaps at higher frequencies for both TE and TM mode. In our modeling we only show one stage of oxidation followed by one step of etching. Consecutive oxidation and etching should produce different gap maps adding more flexibility

to design a silicon PC. Oxidation and etching may be applied as a technique to tune the desired gap frequencies of the defect after the initial device fabrication steps.

4.2 SILICON PHOTONIC CRYSTAL - TRIANGULAR LATTICE OF SILICON PILLARS

This kind of pillar configuration is fairly dominated by TM band gap without the presence of any significant CBG. Fundamental TE gap can be found in higher frequencies for medium r_0/a values. We model our structure for r_0/a =0.2.

4.2.1 Effect of Oxidation

When oxidation is performed in order to grow SiO_2, it hardly affects the TM band gap width as seen from figure 20.
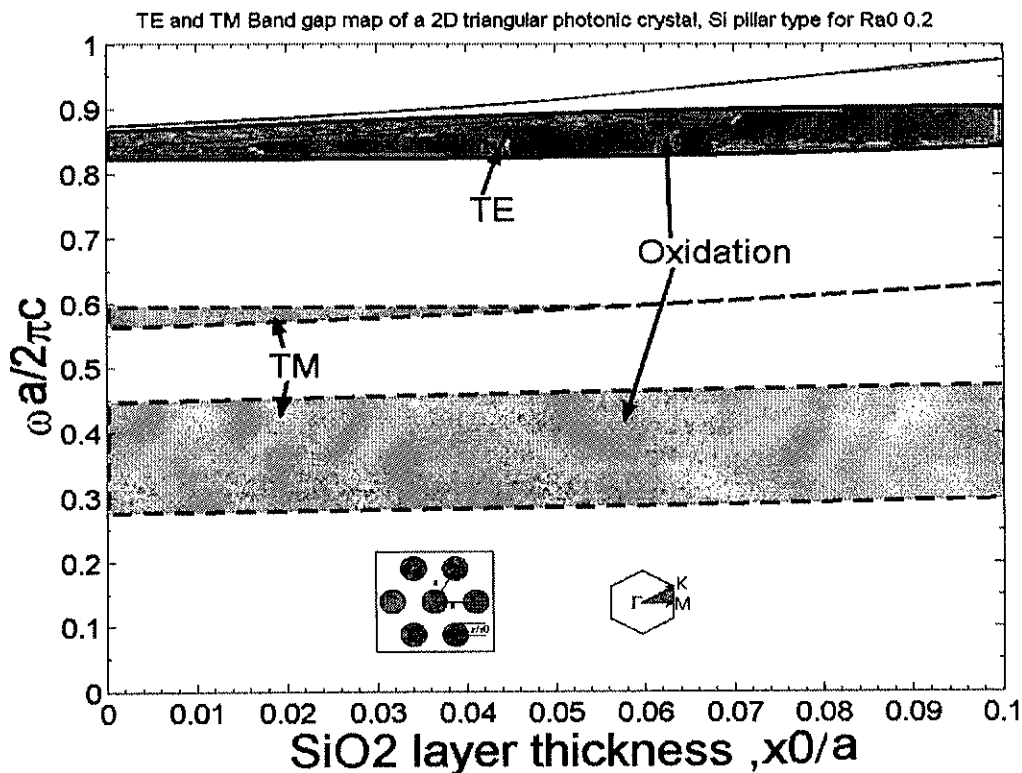
Figure 20. Gap map of the triangular Si pillar 2D PC with increasing SiO_2 layer due to oxidation. Here r_0/a=0.2. Schematic and IBZ for this structure are shown in the inset.

But midgap frequency is increased. For TE mode, gap width increases at a faster rate up to a

certain thickness of SiO₂ with a slower increase in mid gap frequency.

4.2.2 Effect of SiO₂ Etching

When we etch out the SiO₂ layer, TM mid gap frequency keeps increasing, accompanied by

little changes in gap width as shown in figure 21. For TE mode, gap width keeps increasing

until a certain value of x_0/a.
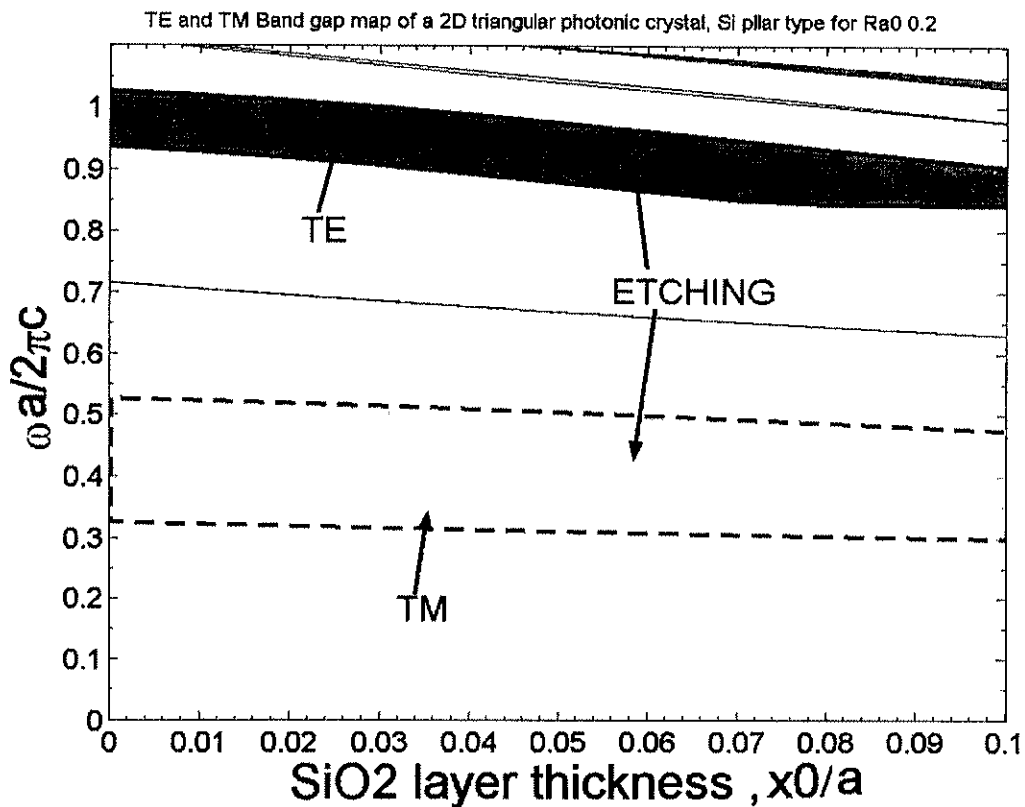
Figure 21. Gap map of the triangular Si pillar 2D PC with decreasing SiO₂ layer due to etching. Here r_0/a=0.2.

Figure 22 shows the gap-midgap ratio for both the TE and TM mode. TM mode has same

lower gap-midgap ratio at higher x_0 for both oxidation and etching from 47.3% at x_0/a=0 to

45.5% at $x_0/a=0.1$. This indicates equal rate of change for both gap width and mid gap ratio during those two processes. At $x_0/a=0$, the TE gap-midgap ratio is 5.15% before oxidation and becomes 6.85% at $x_0/a=0.1$ after oxidation. When we completely etch it out it becomes 9.15%.
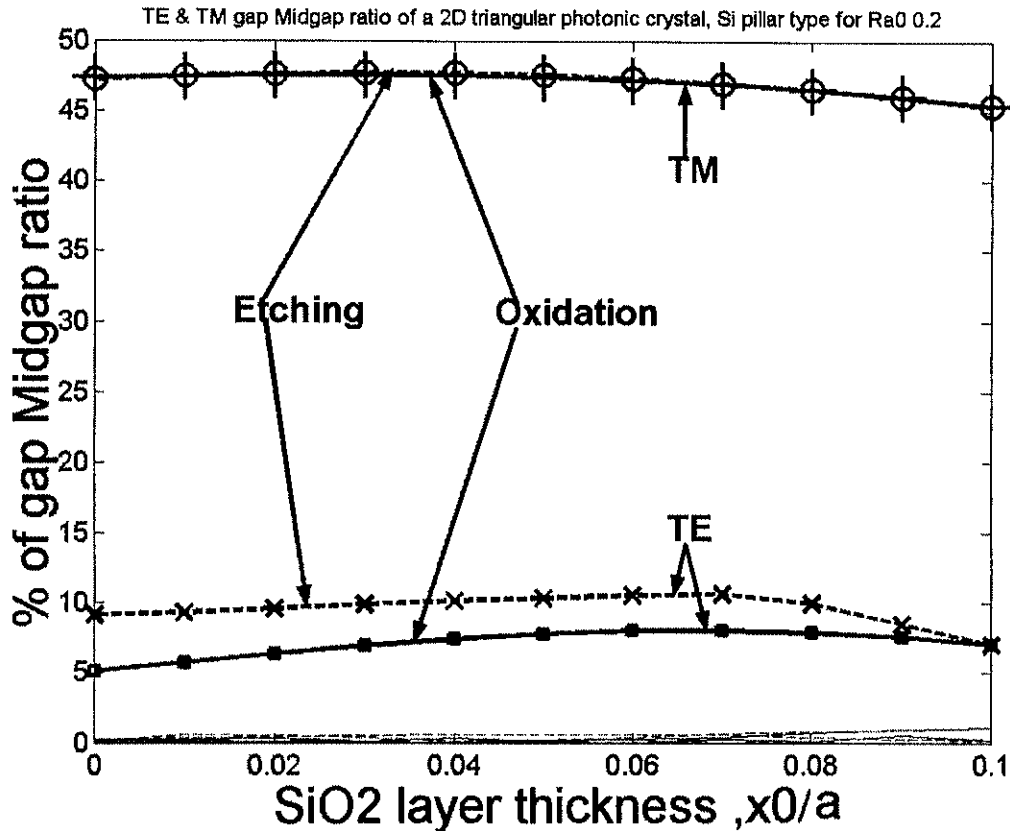
Figure 22. TE and TM gap-midgap ratio triangular Si pillar 2D PC ($r_0/a=0.2$) with decreasing SiO₂ layer after etching, compared with oxidation, began at the SiO₂ layer thickness x_0/a =0.1. The TM gap-midgap ratio is same for both etching and oxidation.

4.3 SILICON PHOTONIC CRYSTAL - SQUARE LATTICE OF AIR HOLES

Like its triangular counter part, the Si 2DPC square lattice with air hole has gap that appears usually at higher r/a. But here the fundamental TM mode gap is significant and appears at lower frequency than the fundamental TE mode gap. We modeled our structure at r_0/a= 0.46, same as in the triangular lattice.

4.3.1 Effect of Oxidation

On oxidation, the TE gap width decreases while the TM gap width increases, see figure 23. The same is true for the cases for higher x_0/a.
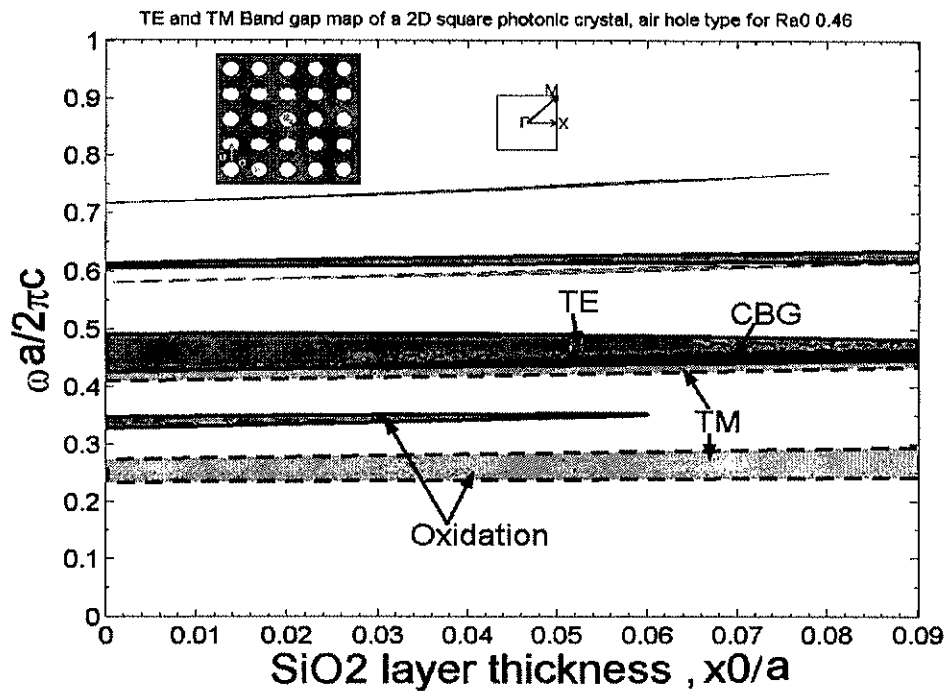
Figure 23. Gap map of the air hole square lattice with increasing SiO_2 layer by oxidation. Notice the CBG at higher x0/a. Here r_0/a= 0.46. Schematic and IBZ for this structure are shown in the inset.

However, mid gap frequency is found to increase in both cases. A narrow complete band gap appears at higher x_0/a due to the overlapping of 2nd TE and TM gaps.

4.3.2 Effect of SiO₂ Etching

The TM gap width increases while that of TE increases on SiO₂ layer etching, after oxidation, see figure 24. The mid gap frequency is found to increase for both modes, as (x_0/a) decreases.
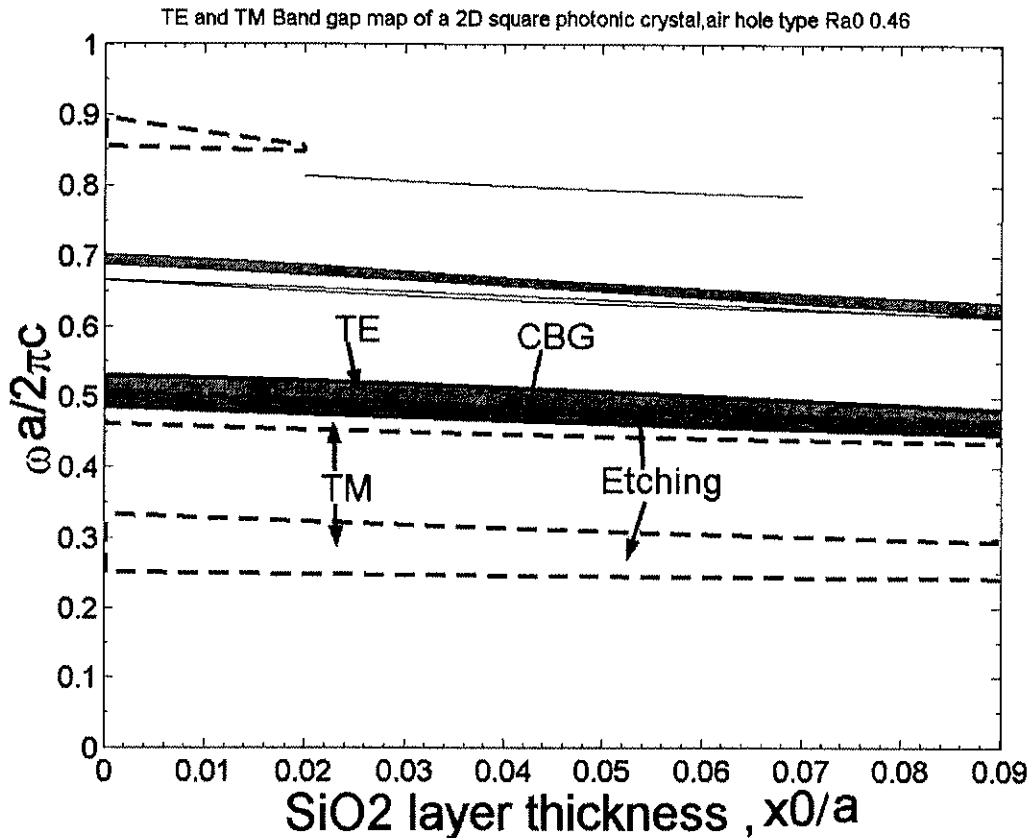
Figure 24. Gap map of the air hole square lattice with decreasing SiO₂ layer due to etching. Here CBG exist trough out the variation of x_0/a.Here r_0/a=0.46

Unlike triangular air hole lattice, the square lattice has larger TM gap-midgap ratio. The fundamental TM gap is 15.6% at the beginning and increases to 19.4% at x_0/a=0.9 after oxidation. After complete etching it becomes 28.2%.Among the TE mode gap, second gap is

the largest. However it becomes the fundamental gap after vanishing of the fundamental one during oxidation. Before oxidation, it was 13.8% and after complete etching, it becomes 8.7%. Other gaps are near 5% or below. See figure 25 for details.
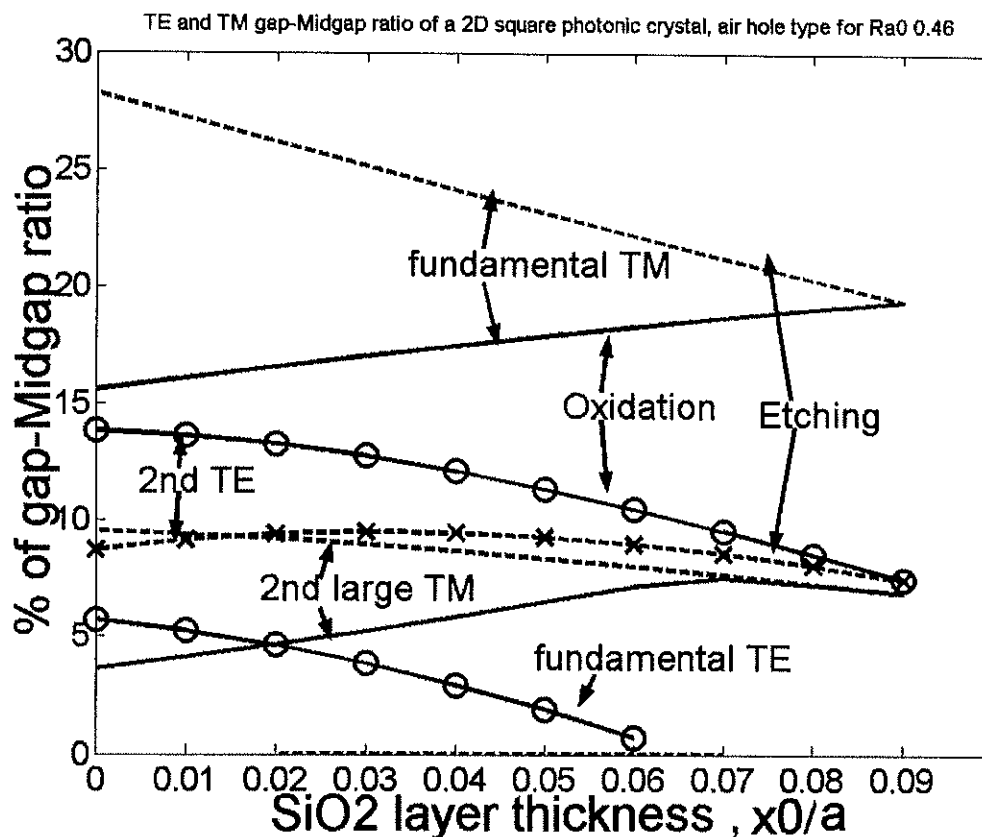
Figure 25. TE and TM gap-midgap ratio of air hole square lattice (r_0/a=0.46) for etching, after oxidation, for SiO_2 layer thickness x_0/a =0.09. Dotted lines indicate the etching, while solid lines indicate the oxidation. Here we have comparable 2nd gap-midgap ratios for both TE and TM modes. The fundamental TE gap vanishes at higher oxidation level and and it is absent during etching. Note that, CBG created during oxidation and etching, is less then 5% and isn't shown in this figure.

49

4.4 SILICON PHOTONIC CRYSTAL – SQUARE LATTICE OF SI PILLAR

As we have seen before, pillar type of configuration is dominated by TM gaps without the presence of any significant CBG. Gaps are usually wider at lower r/a. Fundamental TE gap can be found in higher frequencies for medium values of r_0/a, but it is quite narrow compared to its triangular counter part. We model our structure for $r_0/a = 0.2$.

4.4.1 Effect of Oxidation

Oxidation has no effect on the TM band gap width which remains constant; but midgap frequency increases on oxidation.
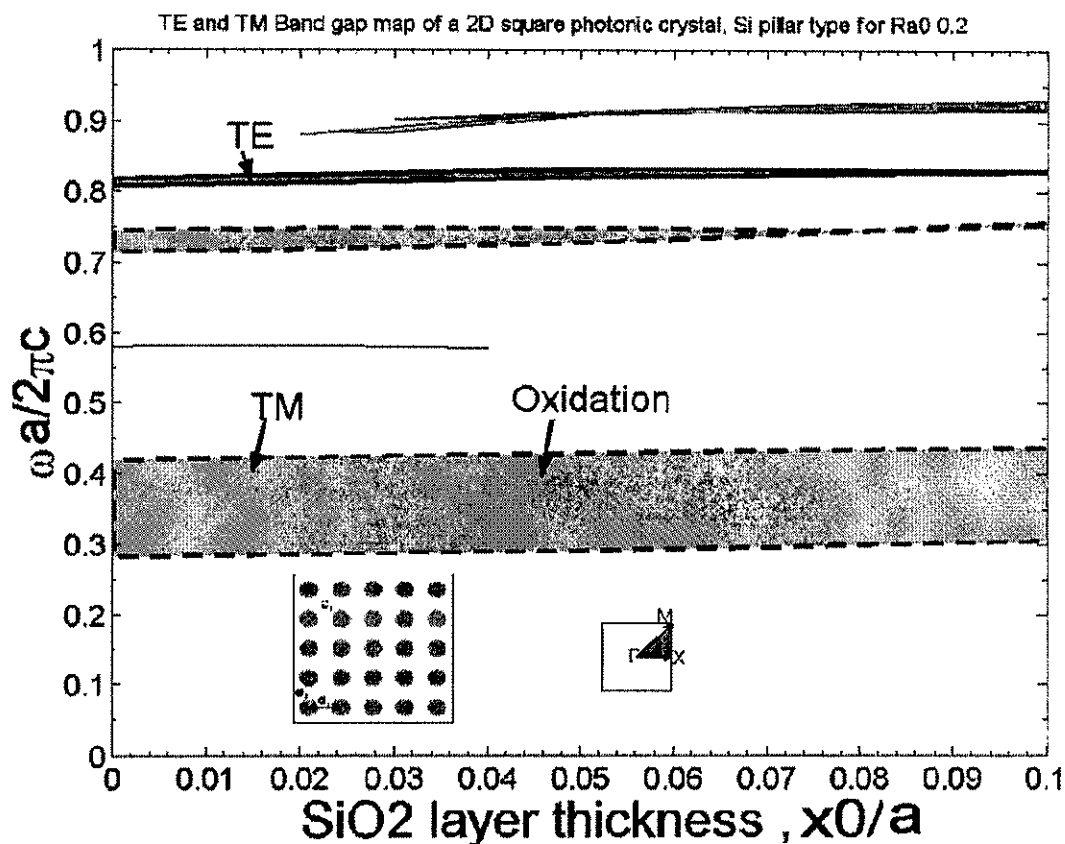
Figure26. Gap map of the square Si pillar PC with increasing SiO_2 layer due to oxidation. Here, $r_0/a=$ 0.2. Schematic and the IBZ are shown in the inset.

For TE mode, the gap width is very insignificant and decreases with the increasing x_0/a, as seen in figure 26.

4.4.2 Effect of SiO₂ Etching

On etching, only the TM mid gap frequency of the fundamental mode is found to increase. A TM gap present during the oxidation vanishes during etching. There is no significant TE mode in this case as seen in figure 27.
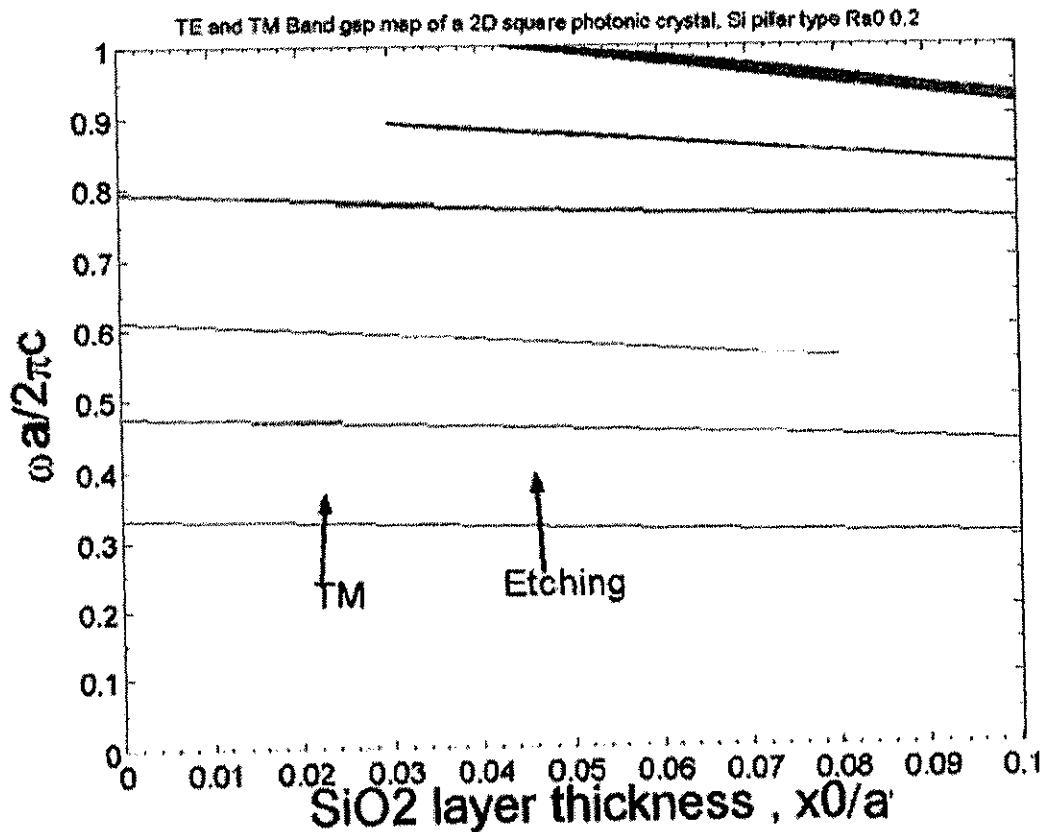
Figure 27. Gap map of the square Si pillar 2D PC with decreasing SiO₂ layer due to etching. Here r_0/a=0.2.

Fundamental TM gap-midgap ratio decreases from 39% to 35.3% at x_0/a=0.1 after oxidation. It becomes 34.8% after complete etching. All other gaps are below 5% (figure 28).
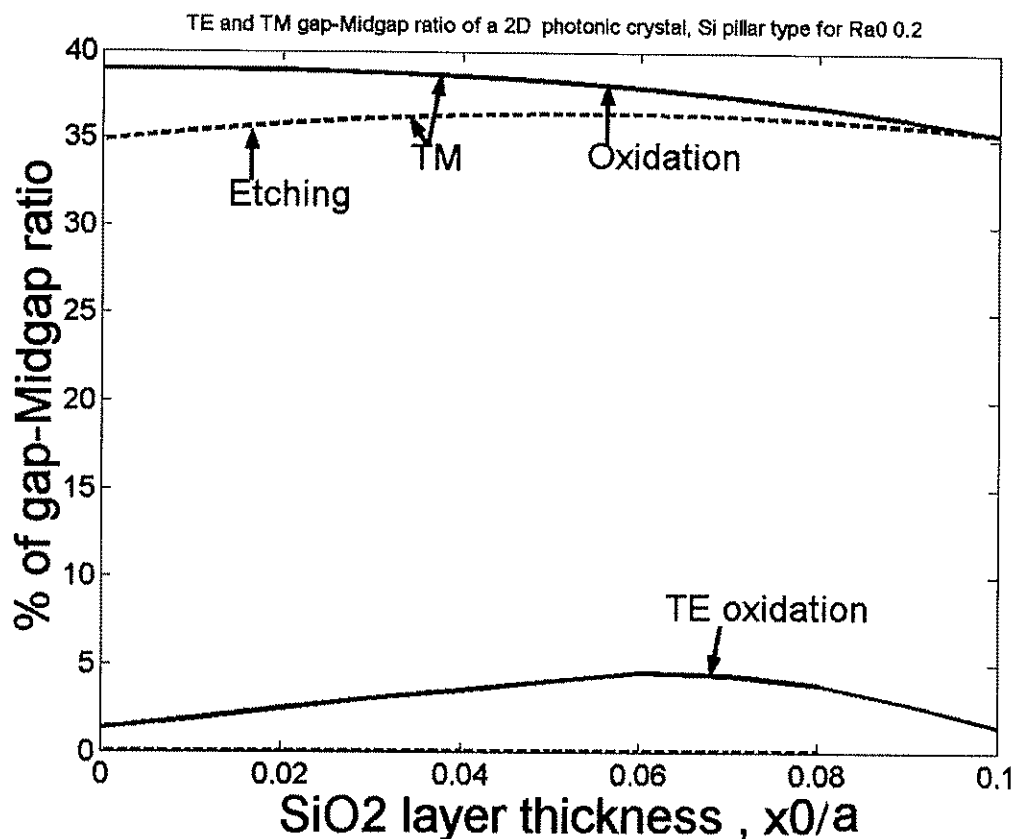
Figure 28. TE and TM gap-midgap ratios of square Si pillar PC (r_0/a= 0.2) with decreasing SiO$_2$ by etching, compared with oxidation to grow SiO$_2$ layer thickness x_0/a= 0.1. There is no significant TE gap-mid gap ratio after etching.

Oxidation and etching are well controlled processes in silicon technology. The effect of time, temperature, ambient, crystal orientation and doping on oxidation are well understood and documented. Hence the results of our study can be easily put into practice for the integration of electronic and photonic devices. There is no oxide layer before oxidation and after complete etching. Therefore, the tuning range of TE and TM band gaps by these two processes is usually limited within the gaps obtained before oxidation and after complete etching.

CHAPTER V

SINGLE DEFECT PBG STRUCTURE

When disorder is introduced into an ideal PBG lattice, localized states are formed in the band gap as those states cannot propagate through the surrounding periodic materials. Using the localization property, practical devices such as microcavities and wave guides can be made with PCs containing defects. Change in any parameters which may affects band structure (see chapter II) in a specific region can be introduced defect mode. This can be the change in size of 'atoms' or change in refractive index contrast. The localized states are analogous to energy states such as donors, acceptors or traps within the band gap of a semiconductor.

Here, we use square lattice pillar structure as our example to introduce a point defect. At first we simulate a single point defect in a Si pillar structure of square lattice. We introduce the defect by enlarging the diameter of the pillar for a single 'atom'. Next, we will oxidize the defect structure and monitor any frequency shift. Then we partially etch out SiO_2 from defect 'atom'. Finally we etch out the SiO_2 layer completely. The final structure becomes same as the original defect with Si pillar of reduced diameter.

Oxidation of Si decreases the average refractive index of the PC. As a rule of thumb, if defect causes the average index of the PC to decrease, the eigen frequency will shift towards a higher value, and one or more bands from the bottom may merge into the band gap, creating so called 'acceptor' defect bands.

As an example, we have a 5x5 square lattice structure of Si pillar $r=0.2a$ and $a =1\mu m$. In the previous chapter we have seen that the band gap for TM mode is in the range of 0.28 to 0.41 for this particular structure. We introduce defect by enlarging the center rod radius to $0.6a$ (upper left corner, figure 29).
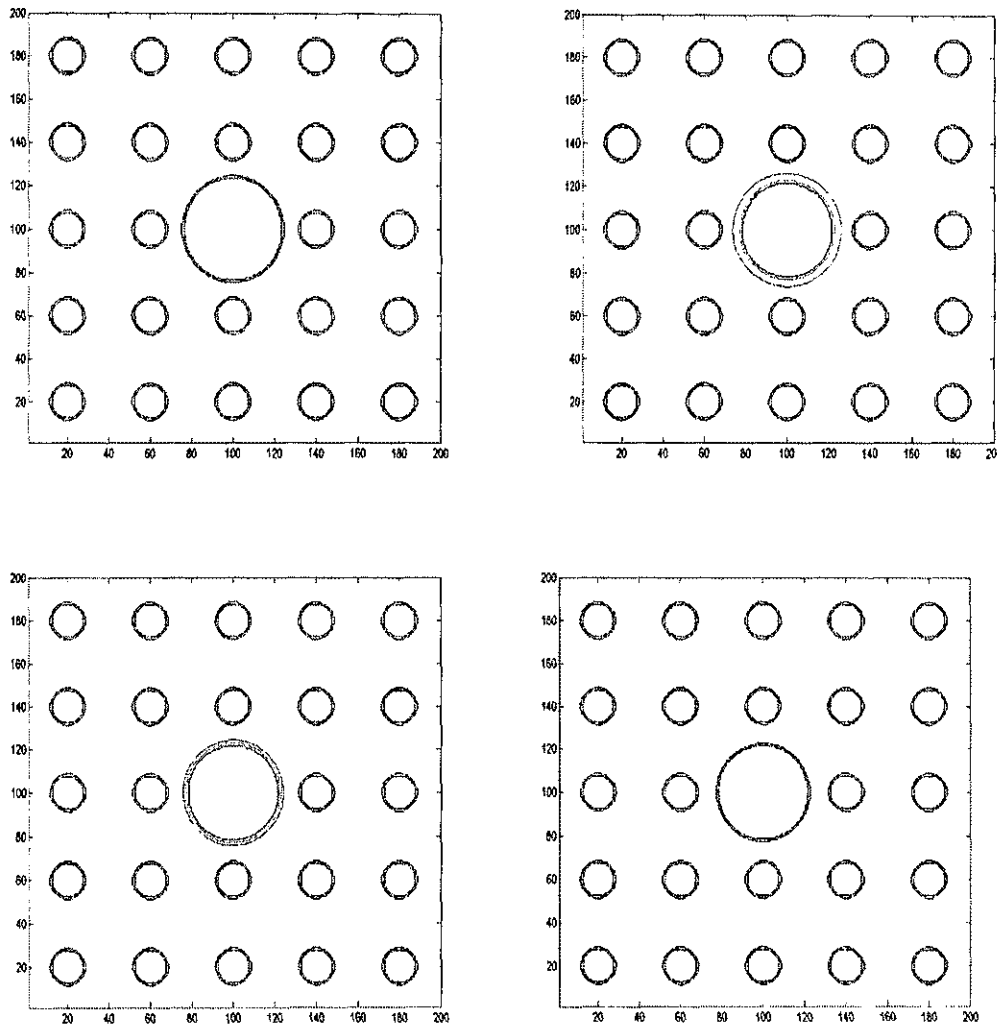
Figure 29. Schematic of different defect structures in a 2D square lattice of Si pillars. Upper left corner: sample defect structure with a center Si pillar of $r=0.6a$. Upper right corner: the defect rod after oxidation, SiO$_2$ thickness $x_0 = 0.1a$. Lower left corner: partially etched SiO$_2$ in the oxidized defect, $x_0=0.05a$, and Lower right corner: after complete etching of SiO$_2$ layer, Si pillar radius $r= 0.55a$. Outer circular ring surrounding the defect circle indicates the perimeter of SiO$_2$ layer in upper right and lower left schematics.

Thus a defect state is formed inside the gap. To identify the frequency response we used a Gaussian source with frequency 1.05e8 Hz. Using FDTD software developed in [30] we have simulated our model. The whole space is discretized in to 200x200 grid, with $\Delta x = \Delta y = 0.025\mu m$, time step $\Delta t = 5.89e\text{-}11 s$ and the number of time steps= 50,000. Number of PML layer used is 10. Then we selectively oxidized only the defect rod (upper right corner, figure 29). We grow a SiO_2 layer of thickness $x_0/a = 0.108a$, slightly larger than $0.1a$. Thus, we get a Si pillar radius $r = 0.55a$. And then we set the thickness of SiO_2 at $0.1a$ by etching. This is because, the space discretization of the grid allows us only those dimensions, integer multiple of Δx. We use the same grid dimension as of [30] in order to verify our result. After oxidation, we etch out the SiO_2 layer partially and then completely (lower left and lower right corner, figure 29). In these cases, x_0 is 0.05a and 0 respectively.

In each case, we monitor the frequency spectrum for the 1st mode. A comparison of the frequency spectrum is shown in figure 30. In each step, we gradually reduce the average refractive index contrast of the PBG structure. These are initially done by, replacing Si with much lower refractive index material SiO_2. And then by partially and completely etching out the SiO_2 layer we lower the average refractive index further. Hence, the frequency spectrum should shift towards the higher frequency according to the rule of thumb. For the original defect the normalized frequency is about 0.329. After oxidation it shifts to 0.34. And it becomes 0.344 and 0.349 after partial and complete etching respectively. These frequency shifts match with the trend of TM gap map profile for square Si pillar 2D PBG structure presented in the previous chapter (figure 26-28).
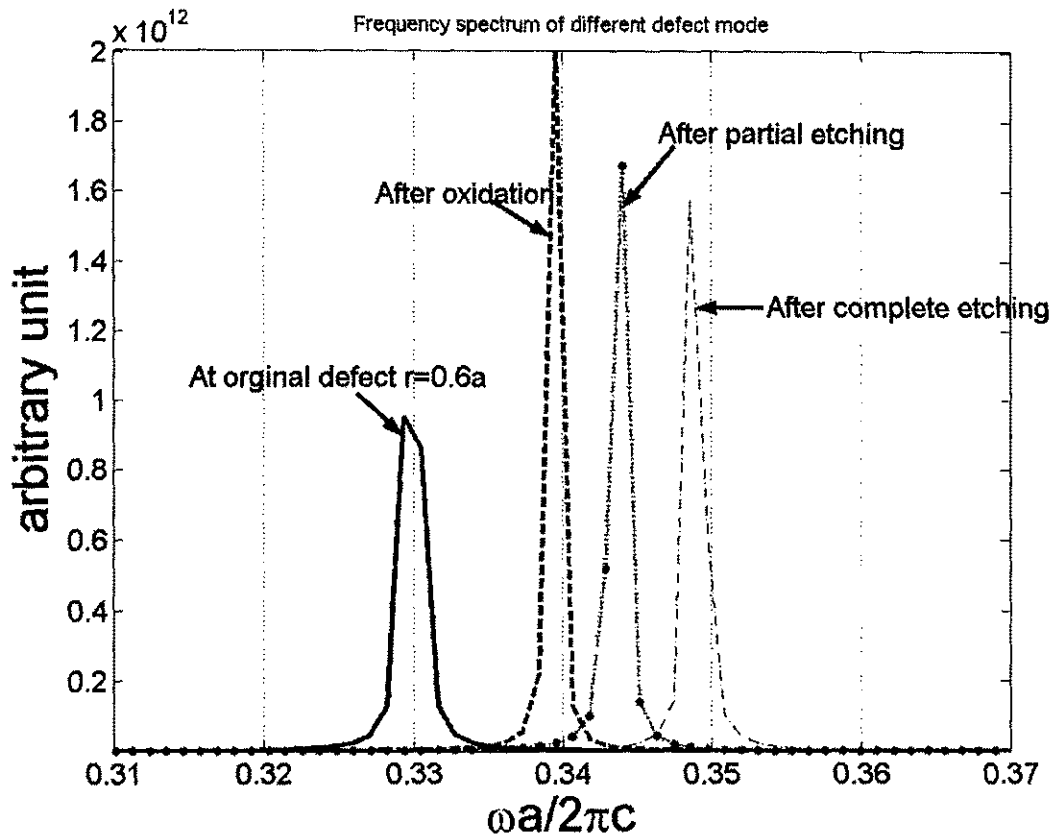
Figure 30. Defect mode frequency spectrum of the four structures shown in figure 29.

These results demonstrate that oxidation and etching are two elegant but simple methods to tune the properties of Si photonic crystals. There are many applications of such microcavity like laser or optical switching devices where tuning is essential for flexible operation. These techniques may provide some easy solutions for those problems.

CHAPTER VI

SUMMARY AND CONCLUSION

Modeling and analysis of silicon photonic crystals have been presented. In particular, the effect of oxidation and etching of 2D Si PC's of triangular and square lattices is examined with a view to integrate CMOS and photonic devices in silicon. The lattices made of air holes and Si pillars were used as sample structures. We have used the plane wave expansion method (PWM) previously developed in the Photonics Lab at ODU for modeling and simulation. Since we are interested only in the 'in plane propagation' of EM wave through the PC, the effect of inserting or removing the SiO_2 layer along the pillars or holes in the (x-y) plane of the structure has been considered. For an untrained eye, oxidation to insert and etching to remove a SiO_2 layer appear to be identical. However, there are subtle differences those affect the properties of the PC. While etching affects the dimension of SiO_2 and air only, oxidation affects the dimensions of all three components including Si. During oxidation, Si is consumed to convert it into SiO_2. The volume of SiO_2 is more than the volume of Si consumed. This leads to two significant effects: first, the Si filling factor decreases producing lower effective dielectric permittivity and second, radius of the air hole or the Si pillar changes even though the lattice constant is unaffected. These two effects will change the properties of the photonic band. Subsequent to oxidation, if we reduce the SiO_2 thickness by etching, the radius and effective dielectric permittivity will be affected, but the lattice constant and Si dimension remain the same. Thus we expect that oxidation and etching will not result in identical effect on the PBG. Hence, etching is not a reversible process of oxidation in terms of changing the band structure of a PC.

In all cases, the band gap of a PC can be varied by SiO_2 grown by oxidation usually within the limits dictated by the (r/a) ratio for initial and final radii of pillar or hole. While etching, the (r/a) ratio does not follow the same path as oxidation and the band gap reverses in a different path. After complete etching of SiO_2, the final (r/a) ratio usually results a higher band gap. For pillar configuration, gap-midgap ratio of TM mode is found decreasing with both increasing oxide thickness during oxidation and decreasing during etching thickness of SiO_2; TE modes behave opposite to TM modes for the same situation. For hole configuration, the results for TE and TM mode usually have opposite trend that of the pillar. However, no systematic variations could be identified; it needs to be calculated separately for each lattice.

We also simulated the effect of oxidation and etching on a single defect in square lattice of Si pillars. First we oxidized the defect rod of a larger diameter; then we partially and completely etched out SiO_2 from the defect surface. Resonance frequency spectrum of the defect gradually shifts to higher values (i.e, blue shift) after each step. Q values of the defect are found to be higher after oxidation and partial etching than the initial value. However, no attempt is made to analyze this or to calculate exact Q values. These could be subjects of future work.

These results demonstrate that oxidation and etching are two elegant but simple methods to tune the properties of Si photonic crystals. In chapter II, we discussed various tuning methods. Several of those methods have dynamic tunability. In non-dynamic tuning, lithographic tuning has wider band gap tunabilty. However that is equivalent to redesigning the PC structure. Oxidation and etching can be used as a post fabrication tuning technique for a Si

PC. Moreover, it does not require a lithography step which is more expensive and cumbersome.

However, in most of the cases, one can also obtain similar tuning results from oxidation and etching, by simply etching the Si layer of a PC to alter (r/a) ratio. Our results show that SiO_2 does not significantly change the 'total band gap map pattern' of a particular PC. But by these methods, it is possible to tune the band gap for a particular (r/a) by changing r alone by oxidation and etching, which do not require a new mask and photolithography. Thus for a fixed pitch and initial radius it is possible to alter the band structure without fabricating it again. During oxidation or etching new higher band gaps are opened for some particular initial r/a. But, in most of the cases, those gaps are available in a higher or lower r/a than the initial value for PC without SiO_2 layer.

The main disadvantage of Si etching is that the amount of Si etching needed to perform the tuning is very fine and hard to control the process in dry etching. On the other hand, our modeling suggests that amount of SiO_2 needed to grow or to etch out is much larger for similar kind of result. And the selectivity of wet etching of SiO_2 over Si is extremely high. Moreover, both oxidation of Si and etching of SiO_2 have higher precision in controlling the thickness of SiO_2 and are already mature technologies in the current semiconductor industry. Hence, one can smoothly control the average refractive index profile of the PC by introducing a third dielectric like SiO_2, hence the band structure, unlike metallic coatings [77].

It is well known that a natural oxide grows on fresh Si surface that is exposed to the atmosphere. Hence, designing a Si PC with SiO_2 layer may also prevent the unwanted change in PBG device characteristics introduced by natural SiO_2 layer. The SiO_2 will serve also as a protective layer for the Si PC.

Our proposition of using SiO_2 in Si PBG structure for design and post processing is simple and compatible with current CMOS technologies. We already have seen silicon PBG waveguide in lasing action [21]. Another potential application of our proposed techniques will be for further tuning of the operational frequency of the laser.

APPENDIX I

RADIUS DETERMINATION

Here, we summarize the dimensional change in PC due to oxidation. Details about oxidation, etching and other electrochemical phenomenon can be found in [10]. During oxidation process 1 mole of Si is consumed to grow 1 mole of SiO_2. For example, 440 nm of silicon is consumed to produce 1000nm of SiO_2 from a planar sample,

$$\frac{\text{Vol. of 1 mol of Si} \times x \text{ mol}}{\text{Vol. of 1 mol of } SiO_2 \times x \text{ mol}} = \frac{\text{Vol. of Si consumed by } SiO_2 \text{ in unit total volume}}{\text{Vol. of SiO2 formed in unit total volume}} \qquad (A1)$$
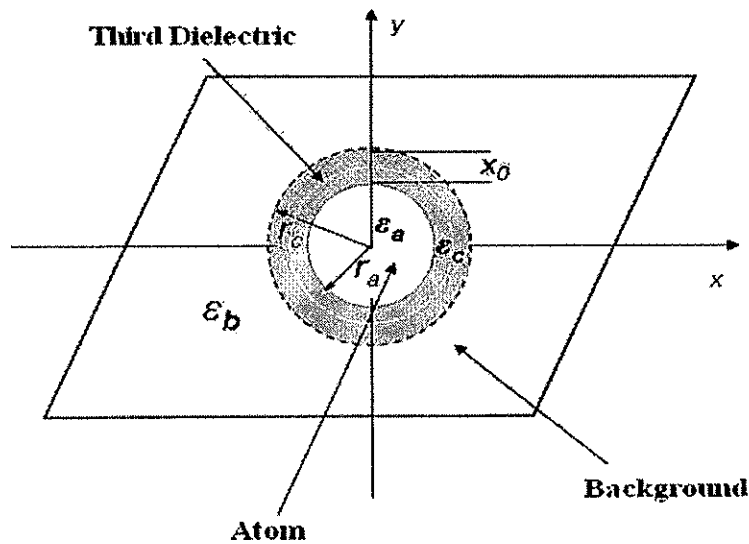
Figure 31. Schematic of the cross section of a unit cell of a possible PBG structure. r_a is the radius of the hole or pillar, x_0 is the thickness of SiO_2, r_c is the combination of r_a and $x0$. The white circle indicates the initial radius of the atom, R_{a0} when $x_0=0$, i.e. $r_c = r_{a,}$. ε_a, ε_b and ε_c are the dielectric constant of the indicated materials. For a pillar configuration Si constitutes 'atom' and in a hole configuration it forms the background.

So, for a cylindrical Si 2D PBG structure with an initial pillar radius 'R_{a0}' and height 'h',

$$\frac{\pi h (R_{a0}{}^2 - r_a{}^2)}{\pi h (r_c{}^2 - r_a{}^2)} = 0.44 \tag{A2}$$

where, ratio of 1mole Si and 1 mol SiO_2 is 0.44. Note that, each radius and distance used here, is normalized with the inter hole spacing or pitch a, e.g. r_c refers r_c/a.

Or,

$$(R_{a0}{}^2 - r_a{}^2) = 0.44(r_c{}^2 - r_a{}^2) \tag{A3}$$

Again,

$$r_c = x_0 + r_a \tag{A4}$$

where, x_0 is the thickness of the SiO_2 layer.

Replacing r_c we can express r_a with x_0 and R_{a0} from equation (A3) and (A4),

$$r_a{}^2 + 0.88 x_0 r_a + 0.44 x_0{}^2 - R_{a0}{}^2 = 0 \tag{A5}$$

Or,

$$r_a = -0.44 x_0 \pm \sqrt{R_{a0}{}^2 - 0.2464 x_0{}^2} \tag{A6}$$

Like wise for a air hole structure equation (A2) become

$$\frac{\pi h (r_c{}^2 - R_{a0}{}^2)}{\pi h (r_c{}^2 - r_a{}^2)} = 0.44 \tag{A7}$$

And by equation (A4) and (A7) we can express r_a,

$$r_a{}^2 + 1.12 x_0 r_a + 0.56 x_0{}^2 - R_{a0}{}^2 = 0 \tag{A8}$$

Or,

$$r_a = -0.56 x_0 \pm \sqrt{R_{a0}{}^2 - 0.2464 x_0{}^2} \tag{A9}$$

With the help of equation (A6) or (A9) depending on structure type and eq (A4), we can

determine PBG for different initial radius R_{a0} and x_0 independently. However, we have to

choose R_{a0} and x_0 in such a fashion, so that those satisfy the constraint, $0 < r_a \leq r_c < 0.5$ in order to maintain a unit cell structure of three materials. Otherwise SiO_2 layer of one cell starts to touch SiO_2 layer of adjacent cell. This situation is not our topic of interest, which could be explored in future work.

choose R_{a0} and x_0 in such a fashion, so that those satisfy the constraint, $0 < r_a \leq r_c < 0.5$ in order to maintain a unit cell structure of three materials. Otherwise SiO_2 layer of one cell starts to touch SiO_2 layer of adjacent cell. This situation is not our topic of interest, which could be explored in future work.

REFERENCES

1. E. Yablonovitch, Scientific American (International Edition), **285,** 47 (2001).

2. P. Yeh, A. Yariv, and C.S. Hong, J. of Opt. Soc. Am., **67,** 423 (1976).

3. E. Yablonovitch, Phys. Rev. Lett., **58,** 2059 (1987).

4. V. P. Vykov, Sov. J. of Quant. Electron. **4,** 861 (1975).

5. J. P. Dowling, Photonic Crystal Bibliography (url, http:// phys.lsu.edu/ ~jdowling/pbgbib.html, last revised: 01 July, 2005)

6. E. Chow, S. Y. Lin, S. G. Johnson and J. D. Joannopoulous, Opt. lett. **26,** 286 (2001).

7. E. Yablonovitch, J. Opt. Soc. Am. B **10,** 283 (1993).

8. S. Y. Lin, E. Chow, V. Hietala, P. R. Villeneuve, and J. D. Joannopoulos, Science **282,** 274 (1998).

9. F. M¨ Uller, A. Birner and U. M. G¨osele, J. Porous Materials **7,** 201 (2000).

10. X.G. Zhang, *Electrochemistry of Silicon and its Oxide* (Kluwer Academic-Plenum Publisher, New York 2001).

11. R. Coccioli, M. Boroditsky, K. Kim, Y. Rahmat-Samii, and E. Yablonovitch, Proc. Inst. Elec. Eng., J. Optoelectron., **145,** 391 (1998).

12. M. Lon˘car, T. Yoshie, A. Scherer, P. Gogna, Y. Qiu, Appl. Phys. Lett., **81,** 2680 (2002).

13. R. K. Lee and O. Painter, J. Opt. Soc. Am., B **17,** 629 (2000).

14. E. R. Brown, C. D. Parker, and E. Yablonovitch, J. Opt. Soc. Amer., B **10,** 404. (1993).

15. P. Kramper, A. Birner, M. Agio, C.M. Soukoulis, F. M'uller, U. Gosele, J. Mlynek, V. Sandoghdar, Phys. Rev., B **64**, 233102 (2001).

16. Y Rahmat-Samii, *"PBG, FSS and Fractal Structures: Analysis, Design and Optimization"* MURI Annual Review Meeting: (URL: http// www. ee.ucla.edu /labs /photon/1999) (accessed date: 10 July 2005).

17. A. Liu, R. Jones, L. Liao, D. Samara-Rubio, D. Rubin, O. Cohen, R. Nicolaescu, and M. Paniccia, Nature, **427**, 615 (2004).

18. M. Meier, A. Dodabalapur, J. A. Rogers, R. E. Slusher, A. Mekis, A. Timko, C. A. Murray, R. Ruel, and O. Nalamasu, J. Appl. Phys., **86**, 3502 (1999).

19. O. Painter and R. K. Lee, Science **284**, 1819 (1999).

20. M. Galli, M. Agio, L.C. Andreani, M. Belotti, G. Guizzetti, F. Marabelli, M. Patrini, P. Bettotti, L. Dal Negro, Z. Gaburro, L. Pavesi, A. Lui, P. Bellutti, Phys. Rev., B **65**, 113111 (2002).

21. . O. Boyraz and B. Jalali, Opt. Express **12**, 5269 (2004).

22. J. D. Jackson, *Classical Electrodynamics,* 3rd edition, (Wiley & Sons, 1998).

23. M. Boroditsky, T. F. Krauss, R. Coccioli, R. Vrijen, R. Bhat, and E. Yablonovitch, Appl. Phys. Lett., **75**, 1036 (1999).

24. S. Fan, P. R. Villeneuve, J. D. Joannopoulos, and H. A. Haus, Optics Express **3**, 4 (1998).

25. G. B. Arfken and H. J. Weber, *Mathematical Methods for Physicists,* Academic Press (1995).

26. S. Fan, P. R. Villeneuve, J. D. Joannopoulos, M. J. Khan, C. Manolatou, and H. A. Haus, Phy. Rev., B**59**, 15882 (1999).

27. J. C. Knight, J. Broeng, T. A. Birks, P. St. J. Russell, Science **282**, 1476, (1998).

28. R. K. Lee, Y. Xu, and A. Yariv, J. Opt. soc. Am. B **17**, 1438 (2000).

29. S. John and T. Quang, Phys. Rev., A **52**, 4083 (1995).

30. S. Guo, Ph. D. Dissertation, Old Dominion University, (2003).

31. S. John and V. Rupasov, Phys. Rev. Lett., **79**, 821 (1997).

32. S. Saltiel and Y. S. Kivshar, Opt. Lett. **25**, 1204 (2000).

33. E. Lidorikis, M. M. Sigalas, E. N. Economou, C. M. Soukoulis , Phys. Rev., B **61**, 13458 (2000).

34. S.Y. Lin, Opt. Lett., **25**, 1297 (2000).

35. S.Y. Lin and J. G. Fleming, J. of Lightwave Tech. **17**, 1944 (1999).

36. K. Busch and S. John, Phys. Rev., E **58**, 3896 (1998).

37. S. Rowson and A. Chelnokov, J.of Lightwave Tech. **17**, 1989 (1999).

38. P. Bettotti, Z. Gaburro, L. Dal Negro, L. Pavesi: J. Appl. Phys. **92**, 6966 (2002).

39. U. Gruninga, V. Lehmann, S. Ottow and K. Busch, Appl. Phys. Lett. **68**, 747 (1996).

40. A. Birner, R.B. Wehrspohn, U. M. G"osele, K. Busch: Adv. Mater. **13**, 377 (2001).

41. M. Born and E. Wolf, *Principle of optics*, (Pergamon, Oxford, 1959).

42. D. Scrymgeour, N. Malkova, S. Kim, and V. Gopalan, Appl. Phys. Lett., **82**, 3176 (2003).

43. K. Yoshino, Y. Shimoda, Y. Kawagishi, K. Nakayama, and M. Ozaki, Appl. Phys. Lett., **75**, 932 (1999).

44. A. Chelnokov, K. Wang, S. Rowson, P. Garoche, J.-M. Lourtioz: Appl. Phys. Lett., **77**, 2943 (2000).

45. A. Blanco, E. Chomski, S. Grabtchak, M. Ibisate, S. John, S.W. Leonard,C. Lopez, F. Meseguer, H. Miguez, J.P. Mondia, G.A. Ozin, O. Toader, H.M. van Driel: Nature **405**, 437 (2000).

46. T. Zijlstra, Drift E van der, M.J.A. de Dood,E. Snoeks, A. Polman, J. Vac. Sci. Tech. B **17**, 2734 (1999).

47. S. Y. Lin, E. Chow, S. G. Johnson, J. D. Joannopoulos, Optics Letters, **25**, 1297 (2000).

48. T. Tada, V.V. Poborchii, T. Kanayama, Jpn. J. Appl. Phys., **38**, 7253 (1999).

49. V. Grigaliunas, V. Kopustinskas, S. Meskinis, M. Margelevicius, I. Mikulskas, R. Tomasiunas, Opt. Mater., **17**, 15 (2001).

50. O. Hanaizumi, Y. Othera, T. Sato, S. Kawakami: Appl. Phys. Lett., **74**, 777 (1999).

51. M. Plihal, A.A. Maradudin: Phys. Rev., B **44**, 8565 (1991).

52. T.F. Krauss, R.M. De La Rue: Progress in Quantum Electronics, **23**, 51 (1999).

53. J. D. Joannopoulos, R. D. Meade, and J. N. Winn, *Photonic Crystals: Molding the Flow of Light,* (Princeton University Press, Princeton, 1995).

54. C. M. Soukoulis, Proc. of the NATO ASI on Photonic Band Gap Materials, Elounda, Crete, Greece, June 18-30, 1995 (NATO ASI Series, Kluwer Academic Publishers, The Netherlands, 1996).

55. R. D. Meade, O. Alerhand, J. D. Joannopoulos: *Handbook of Photonic BandGap Materials* (JAMteX I.T.R. 1993).

56. X. Zhang, Z. Q. Zhang, and L. M. Li, Phys. Rev., B **61**, 1892 (2000).

57. C. Jin, X. Meng, B. Cheng, Z. Li, and D. Zhang, Phys. Rev., B **63**, 195107 (2001).

58. X. Zhang, Z.-Q. Zhang, and C.T. Chan, Phys. Rev., B **63**, 081105 (2002).

59. K. Sakoda: *Optical Properties of Photonic Crystals* (Springer Verlag, Berlin 2001).

60. K. M. Leung, "Plane wave calculation of photonic band structures" in *Photonic band gaps and localizations*, C. M. Soukoulis. ed. (Plenum Press NY 1993).

61. K. M. Ho, C. T. Chan, and C. M. Soukoulis, Phys. Rev. Lett., **65**, 3152 (1990).

62. R. D. Meade, A. M. Rappe, K. D. Brommer, and J. D. Joannopoulos, Phys. Rev, B **48**, 8434 (1993).

63. S. Guo and S. Albin, Optics Express, **11**,167 (2003).

64. K. Bush, C.R. Physique **3**, 53 (2002).

65. I.B. Divliansky, A. Shishido, I.C. Khoo, T.S. Mayer, D. Pena, S. Nishimura, C.D. Keating, and T. Mallok, Appl. Phys. Lett., **79**, 3392 (2001).

66. T. Kondo, S. Matsuo, S. Juodkazis, and H. Misawa, Appl. Phys. Lett., **79**, 725 (2001).

67. T.F. Krauss, R.M. De La Rue, Progress in Quantum Electronics **23**, 51 (1999).

68. M. Loncar, D. Nedeljkovic, and T.P. Pearsall, Appl. Phys. Lett., **77**, 1937 (2000).

69. H. Ohji, P.J. French, S. Izuo, and K. Tsutsumi, Sensors and Actuators **85**, 390 (2000).

70. A. Figotin and Y. A. Godin Ilia Vitebsky, Phys. Rev., B **57**, 2841 (1998).

71. S. W. Leonard, J. P. Mondia, H. M. van Driel, O. Toader, K. Busch, A. Birner, U. Gösele, V. Lehmann and S. John, Phys. Rev., B **61**, 2389 (2000).

72. M. Eich1, M. Schmidt, U. Hübner, R. Boucher,(url:cmp.ameslab.gov/PECSVI/ PECSVIOralContributionsAbstracts/eich.pdf) (accessed date:11 July 2005)

73. K. Yoshino, Y. Shimoda, Y. Kawagishi, K. Nakayama, and M. Ozaki, Appl. Phys. Lett., **75**, 932 (1999).

74. S. Kim and V. Gopalan, App. Phys. Lett., **78**,. 3015 (2001).

75. W. Park, J. B. Lee, App. Phys. Lett., **85**, 4845 (2004).

76. O. Painter, A. Husain, A. Scherer, P. T. Lee, I. Kim, J. D. O'Brien, and P. D. Dapkus, IEEE Phot. Tech. Lett., **12**,1126 (2000)

77. V. Poborchii, T. Tada, and T. Kanayama, A. Moroz, App. Phys. Lett., **82**, 508 (2003).

VITA

G. M. Haider Ali

Education

- Masters of Science in Electrical Engineering
  Old Dominion University, Norfolk VA, USA, 2005.

- Bachelor of Science in Electrical & Electronic Engineering
  Bangladesh University of Engineering and Technology (BUET), Dhaka.
  Bangladesh, 2002.

His main research interests are in theory and simulation on photonic devices, fiber optics and electromagnetics.

Research & Publications

BS project topic-Stimulated RAMAN Scattering in Optical WDM System.
- Model Analysis.
- Improved model proposition.
- Performance evaluation and Statistical Analysis.

Regarding Conference publications:
- ICCIT-2001, December, University of Dhaka, Bangladesh.
- 2nd ICECE-2002, December, Pan Pacific Sonargaon Hotel, Dhaka, Bangladesh.